ACS Biomaterials SCIENCE & ENGINEERING

pubs.acs.org/journal/abseba

Review

Extrusion-based 3D (Bio)Printed Tissue Engineering Scaffolds: Process−Structure−Quality Relationships

Samuel Gerdes, Srikanthan Ramesh, Azadeh Mostafavi, Ali Tamayol,* Iris V. Rivero,* and Prahalada Rao*

Cite This: https://doi.org/10.1021/acsbiomaterials.1c00598

Read Online

ACCESS | Metrics & More | Article Recommendations

ABSTRACT: Biological additive manufacturing (Bio-AM) has emerged as a promising approach for the fabrication of biological scaffolds with nano- to microscale resolutions and biomimetic architectures beneficial to tissue engineering applications. However, Bio-AM processes tend to introduce flaws in the construct during fabrication. These flaws can be traced to material nonhomogeneity, suboptimal processing parameters, changes in the (bio)-printing environment (such as nozzle clogs), and poor construct design, all with significant contributions to the alteration of a scaffold's mechanical properties. In addition, the biological response of endogenous and exogenous cells interacting with the defective scaffolds could become unpredictable. In this Review, we first described extrusion-based Bio-AM. We highlighted the salient architectural and mechanotransduction parameters affecting the response of cells interfaced with the scaffolds. The process phenomena leading to defect formation and some of the tools for defect detection are reviewed. The limitations of the existing developments and the directions that the field should grow in to overcome said limitations are discussed.

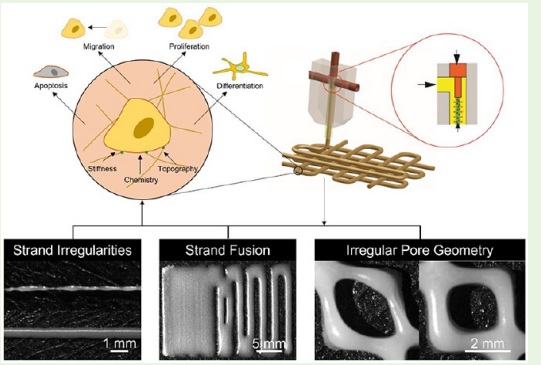

KEYWORDS: *Bio-AM, scaffolds, defects, material rheology, 3D printing, tissue engineering*

1. INTRODUCTION

Biological additive manufacturing (Bio-AM) has garnered growing attention in recent years due to its potential to create tissue engineering scaffolds with fine resolutions and architectural features that mimic native tissue. Bio-AM fabrication falls into two main categories: (1) bioprinting, the printing of biomaterials that have been seeded with cells and (2) 3D printing, the acellular deposition of biomaterials. Within Bio-AM, there are several (bio)printing modalities: extrusion-based, inkjet, stereolithography, and laser-assisted (bio)printing, each featuring distinctive advantages and limitations.

Among various 3D (bio)printing systems, extrusion-based (bio)printing (EBB) has emerged as a popular platform both from a research and application perspective. EBB is a fabrication process based on applying pneumatic or mechanical pressure to the (bio)ink in a syringe-like container to force it out through a nozzle/tip. During extrusion, the print head is moved around the print platform, controlling the deposition pattern of the (bio)ink in 3D.[1] After deposition, the print material should maintain its geometry to preserve the architectural features of the fabricated scaffold. Unlike some of the other (bio)printing methods, EBB is capable of supporting all the primary forms of cross-linking; photo, chemical, and thermal.[2,3] An advantage of EBB systems is their ability to fabricate fibrillar architectures with anisotropic characteristics mimicking those observed in musculoskeletal tissues.[4−6]

Although EBB systems have inferior feature resolution in comparison to their counterparts, these systems can fabricate scaffolds with clinically relevant dimensions significantly faster than other processes and are therefore amenable for scalability. They also are very robust in the 3D (bio)printing of multicomponent scaffolds as it is feasible to switch between materials or cells during the (bio)printing process.[7,8] EBB systems have been developed to add extra levels of structural complexity within the fabricated scaffolds. For example, with coaxial nozzles, hollow filaments have been fabricated, allowing for better transport of nutrients throughout the formed scaffolds. Coaxial nozzles have also led to core−shell fibers, which have realized a method of coculturing. In addition,

Received: May 3, 2021
Accepted: August 20, 2021

Table 1. Scaffold Defect Types, Sources, and Impacts Present in the Extrusion-Based (Bio)Printing Process

Defect	Example	Sources	Impact
Undesirable Strand Diameter	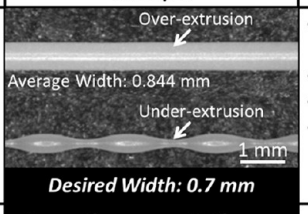	• Suboptimal process parameters • Gelation/crosslinking degree • Material composition • Material rheological properties	• Incorrect scaffold dimensionality • Reduced resolution • Strand fusion • Pore closure
Non-homogeneous Strands	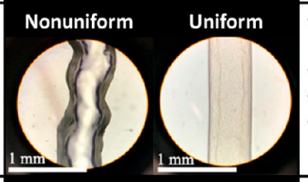	• Suboptimal process parameters • Gelation/crosslinking degree • Material composition • Material rheological properties	• Incorrect scaffold dimensionality • Pore closure
Strand Fusion	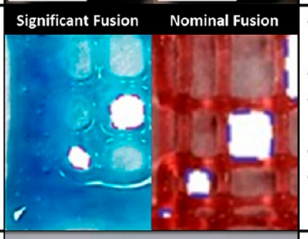	• Suboptimal process parameters • Gelation/crosslinking degree • Material rheological properties • Scaffold design • Material composition	• Pore closure • Incorrect scaffold dimensionality
Strand Collapse		• Suboptimal process parameters • Gelation/crosslinking degree • Scaffold design • Material composition	• Inter-layer pore closure • Insufficient print area for the next layer • Incorrect scaffold dimensionality
Variability in Pore Geometry	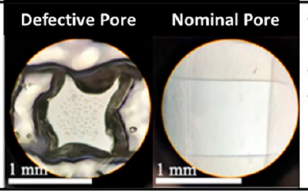	• Suboptimal process parameters • Gelation/crosslinking degree • Material composition	• Pore closure • Incorrect scaffold dimensionality

Figures reproduced with permissions from the top to bottom row: ref 15, Copyright 2020, Mary Ann Liebert, Inc.; ref 16, Copyright 2019, American Chemical Society; ref 17, Copyright 2018, Multidisciplinary Digital Publishing Institute; ref 18, Copyright 2018, Elsevier; ref 16, Copyright 2019, American Chemical Society.

filaments with textured surfaces have been printed that can direct cellular organization. Further, structurally anisotropic fibrillar structures with aligned fibers have been shown to direct cellular organization, function, and migration.[9−11] In unprinted fibrillar scaffolds created by Zhang et al., the fibers facilitate strong cell alignment in cardiomyocytes, likely due to the emulation of natural structures in muscular and nervous tissues.[9] Because of the benefits of anisotropic fibrillar structures, fabrication methods have also been developed for EBB systems. Specifically, specialized Kenics static mixers were designed to mix two hydrogel streams to create internal microfilaments to aid in myoblast maturation.[11] EBB systems can also become portable if needed. Recently, hand-held EBB systems have been developed that allow direct in vivo printing of scaffolds.[12]

Despite the significant advancement of EBB systems in terms of their resolution, speed, compatible (bio)inks, and the level of achievable structural complexity, they are not perfect. In EBB systems, defects are determined as deviations of the physically (bio)printed scaffolds from the intended designs. Various defect types have been characterized (see Table 1) and can originate from the printing process parameters, material composition, level of cross-linking, and other material or process-based variables. Notably, defects can also propagate other defect types, leading to major printability problems. Further, the effect of defects on material printability has been explored in extensively, but the impact of defects on cell response is not thoroughly researched in the literature. While printability analysis has been explored comprehensively elsewhere,[8,13,14] this Review serves to broaden print quality discussions into biological, mechanical, and process quality topic areas in order to provide a more holistic assessment of (bio)printed tissue scaffold quality.

The structure of this Review is as follows: Section 2 summarizes the salient architectural and mechanotransduction parameters affecting the response of cells interfaced with the scaffolds. Section 3 elucidates the link between rheological properties of the material on flaws formation. Section 4 provides strategies used for modulating these rheological properties to ensure flaw-free fabrication. Section 5 summarizes research quantifying the effect of flaws on mechanical properties. Section 6 focuses flaws formed in the EBB process

https://doi.org/10.1021/acsbiomaterials.1c00598
ACS Biomater. Sci. Eng. XXXX, XXX, XXX−XXX

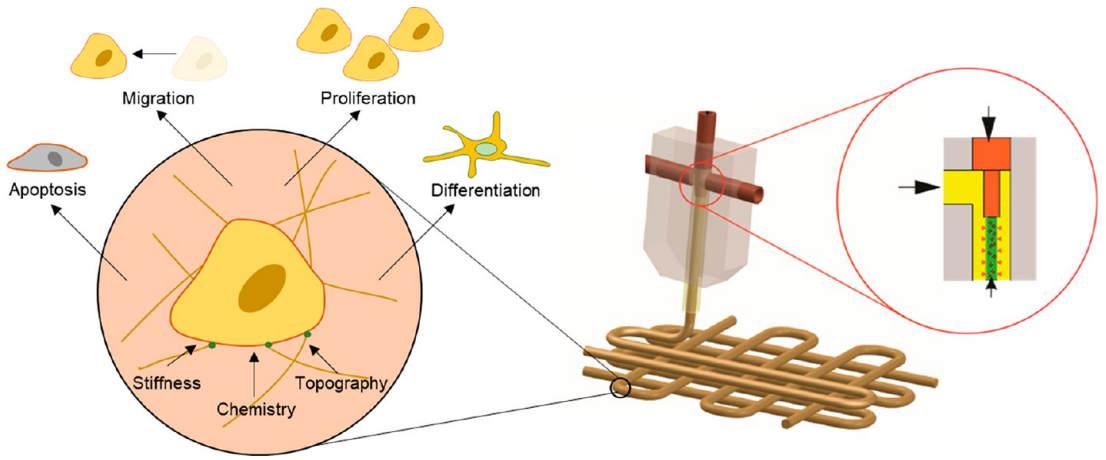

Figure 1. Mechanisms that cells interact with in 3D (bio)printed scaffolds and the biological effects of these interactions.

and discusses flaw mitigation strategies. Lastly, in section 7, a roadmap to overcome and mitigate the barriers caused by defect formation is presented in the conclusions.

2. EFFECT OF GEOMETRICAL FEATURES AND SCAFFOLD PHYSICOCHEMICAL PROPERTIES ON CELLULAR FUNCTIONS

The native cell's environment in the body is a 3D hierarchical multiscale construct consisting of large proteins, such as collagen, laminin, and other molecules known as the extracellular matrix (ECM).[15] The ECM not only provides structural and biomolecular support for cells but also assists in keeping cells in contact with each other and generates a frame for keeping cells together as a larger scale construct (tissue). The type and concentration of macromolecules in the ECM varies by tissue and defines the ranging mechanical properties from soft to hard tissues.

The study of the ECM nano- and microstructures has become more popular since the discovery that cells could sense their environment and respond through contact guidance phenomenon. Contact guidance refers to the cells sensing their environment through membrane receptors and stress fibers (actin bundles) and reacting to these signals by regulating their morphology, migration, and function, which leads to tissue organizations.[16,17] Cell−ECM interactions could explain the different behavior of cells in both in vitro and in vivo situations.[18] These observations have inspired researchers to design the ECM mimicking materials and structures to provide biological, chemical, topographical, and mechanical properties similar to the cell's native environment to direct their response (see Figure 1) in tissue-engineered scaffolds.[19,20]

However, engineered tissue constructs do not capture the sophisticated biological, chemical, and physical properties of native tissues. In addition, small changes in the properties of the scaffolds can affect cell response.[21] For example, defects in the continuity of the properties of the scaffolds can be translated into a discontinuity in the response of the cultured cells, negatively impacting the tissue function. This section discusses the linkages between substrate topographical and mechanical factors and the cellular responses regardless of the fabrication process used for scaffold production. The discussions in the next subsections serve as the basis for future research on improving the predictability and regulating cellular responses within the scaffolds formed with extrusion-based (bio)printing.

2.1. Cell Response to Topographical Signals. Scaffold surface topography is an essential cue to the endogenous or exogenous cells interfaced with the construct. Cells respond to topographical cues, and their response depends on several factors, such as feature shape, size, depth, and cell type.[22,23] A considerable amount of literature has been published on the effect of these topographical features on cell responses and is reviewed comprehensively elsewhere.[22,23] Generally, surface patterns can be categorized into surfaces, grooves, tubes, fibers, pits, pores, pillars, spherical and aspherical micro- to nanotopographies. In this section, these surface topographies that could affect cell responses, such as cell adhesion, migration, proliferation, and differentiation are summarized.

2.1.1. Cell Adhesion. Integrin is a transmembrane receptor protein that plays an important role in adhering cells to each other and to the ECM.[24] Notably, any cell detectable changes in the surface can affect integrin expression and cell adhesion to the surface. One example of a cell detectable change is the relationship between nanoscale surface random roughness and cell adhesion. In rat neuron cell culturing experiments, adhesion was maximized when the average surface roughness (R_a) was between 20 and 100 nm.[25,26]

A nanofibrous substrate, such as electrospun sheets, has also demonstrated increased cell adhesion compared to flat surfaces.[27,28] Mainly, surfaces with grooves and ridges with pitch dimensions of 400−1200 nm showed a higher ability for cell attachment, and cells displayed higher shear resistance as a result, as opposed to flat surfaces.[29]

The study of nanoparticles and nanodots on substrate surfaces revealed that the size and space between deposited features has a consequential effect on cell attachment.[30,31] Goreham et al. created a gradient of nanotopography by controlling the organization of nanoparticles with three diameters of 16, 38, and 68 nm. Cultured osteoblast cells on these substrates demonstrated that cell adhesion decreased with increasing particle size, especially at a 68 nm diameter.[30]

In another study, adhesive gold nanodots with <8 nm diameter were created to facilitate one integrin bind per dot, and dots were positioned at different spacings of 28, 58, 73, and 85 nm.[31] Cultured MC3T3-osteoblasts on these substrates revealed that having ≥73 nm spaces between cells would reduce the cell attachment due to a reduction in integrin clusters and focal adhesion between cells and dots.[31] Gulati et

https://doi.org/10.1021/acsbiomaterials.1c00598
ACS Biomater. Sci. Eng. XXXX, XXX, XXX−XXX

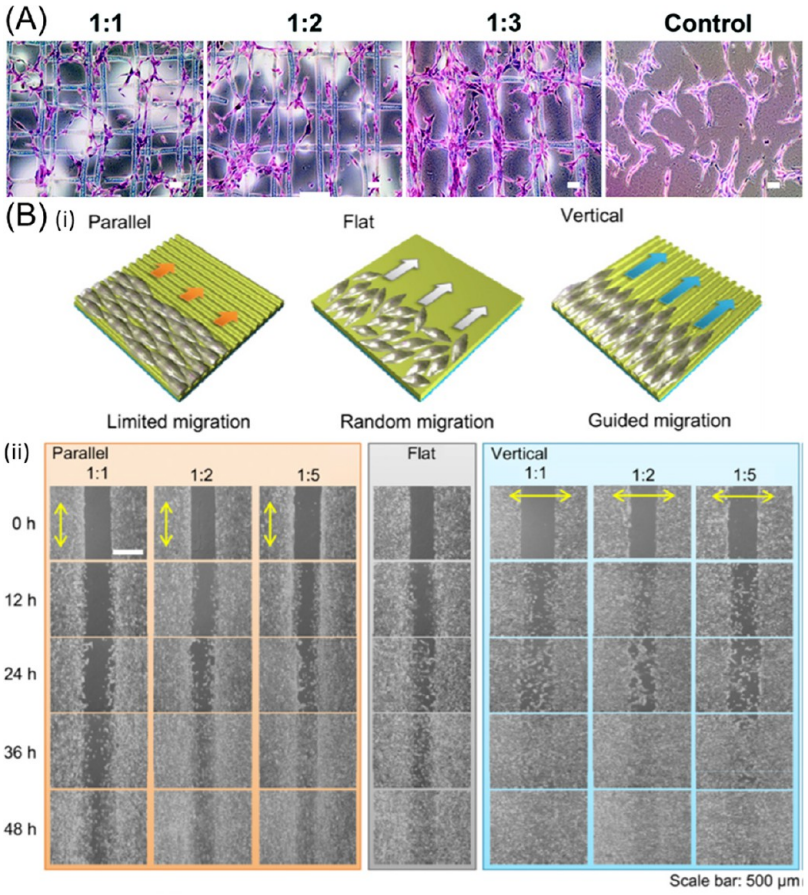

Figure 2. Cell response to topographical signals. (A) Liu et al. examined different cell adhesion and alignment in response to different aspect ratios of printed filaments. Reproduced with permission from ref 45. Copyright 2017, The Royal Society of Chemistry. (B) Cell migration with respect to surface topographical features. (i) Schematic of cell migration behavior in response to surface nanogroove orientation. (ii) Microscopic images of cultured cells on three different surfaces, which facilitated or limited their migration. Reproduced with permission from ref 47. Copyright 2012, Elsevier.

al. 3D printed implants with nano- and microscale topography to improve their surfaces, which increased cell attachment and differentiation.[32]

2.1.2. Cell Morphology, Spreading, and Alignment. After cells adhere to the surface of the substrate, they adapt themselves by changing their morphology, spreading, and alignment. The effect of topography on cell behavior was investigated by patterning nanoislands with three different heights of 15, 35, and 95 nm on the substrate. By decreasing the nanoisland height, cells tended to spread more on the nanoisland features and showed organized cytoskeletal fibers, especially at a 13 nm height.[33] In another group's research, focused on mimicking the myocardium tissue structure, PEG hydrogel nanoscale grids were made with width × gap × height ranges between 150 × 50 × 200 nm, and 800 × 800 × 500 nm, and rat myocytes were cultured on them. Cells were more aligned on the patterned substrates than on flat substrates and were also more spread on the larger patterns (800 × 800 × 500 nm).[34]

To examine the effect of pit topographies on osteoblast cells, Lim et al. prepared nanopit structures (14, 29, and 45 nm deep pits) for culture with human fetal osteoblastic (hFOB).[35] Lim et al. revealed that osteoblasts spread more on shallow pits (14 and 29 nm) than on the deeper pits (45 nm).[35] Moreover, cells can be aligned along the grating axis direction based on the topographical structure. Different diameters (30, 50, 70, and 100 nm) of TiO_2 nanotube arrays were used to investigate their effect on cell behavior. Cultured human mesenchymal stem cells (hMSCs) on these arrays exhibited significant (10-fold) elongation on the larger nanotubes (70 and 100 nm diameter), which induced cells to differentiate into osteoblast-like cells.[36]

In another work, Kim et al. cultured hMSCs on nanogratings with 250 nm width and proved that cells align to specific patterns; however, cells cultured on the nanopatterned surface displayed spread morphology. Furthermore, the aligned cells on the patterned substrate expressed neurogenic and myogenic markers.[37] Aligned electrospun fiber meshes with different diameters (80−740 nm) have also been examined to evaluate cell elongation along the fibers, and the results revealed that the highest cell alignment happened on fibers with a diameter larger than 100 nm.[38]

In a pioneering study, human corneal epithelial cells were cultured on substrates with nanoscale grooves of different sizes. The study revealed that cell orientation could change by pitch patterns.[39] While a perpendicular orientation of cells was observed in patterns with a smaller pitch (400 nm), a parallel orientation was observed by increasing the pitch sizes to 4000 nm. Also, cultured cells on the pitch sizes between 800 and 1600 nm displayed random orientations.[39] Bhuthalingam et al. used a specialized 3D bioprinting technique consisting of making etches on polystyrene with a sharpened needle and

https://doi.org/10.1021/acsbiomaterials.1c00598
ACS Biomater. Sci. Eng. XXXX, XXX, XXX−XXX

depositing (bio)ink in the created grooves. Cultured cells adhered to the substrate, proliferated, aligned, and differentiated in the grooves in a predictable fashion.[40] In another work, Liu et al. used electrohydrodynamic jet (E-jet) 3D printing technology to print different aspect ratios of 1:1, 1:2, and 1:3 from poly(lactic-*co*-glycolic acid) (PLGA) solution and cultured fibroblast on the constructs to evaluate the cell behaviors to the constructs.[41] Liu et al.'s results indicated that cells show different adhesion and alignment in regard to the different aspect ratios (Figure 2A).[41]

2.1.3. Cell Migration. Cell migration is essential to numerous physiological processes, such as skin cell renewal, immune responses, stem cell homing, angiogenesis, and morphogenesis.[42] In examining the effect of surface topographical cues on cell migration, Kim et al. created nanogroove surfaces with 550 nm width and spacings of 550, 1100, and 2750 nm. Cultured 3T3 cells on the patterned surfaces demonstrated that cell migration speed was higher in surfaces with 550−1100 nm spacing in comparison to 2750 nm.[43] Additionally, Kim et al. examined the effect of vertical and parallel patterns on the migration speed of cells cultured on the patterned surfaces. The results suggested that the migration speed of cells was faster on the vertical patterns (Figure 2B).[43] Another study by Kim et al. showed that pattern density could affect cell migration.[44] This study created a lattice pattern with different local densities and cultured 3T3 fibroblasts on the substrate. At first, it was observed that cells were attached to all parts of the surface, but after 14 h passed, cells were moved significantly toward the denser areas of the pattern.[44]

The effect of asymmetric microgeometry on cell migration was explored in a study by Mahmud et al. In the study, different micropatterns such as connected-triangles and lines-with-spikes ratchets were fabricated and cultured with different cell lines, including cancer cells. Mahmud et al. revealed that the geometrical patterns could induce cell polarization and stimulate them to move forward or backward, depending on their lineage.[45] To improve the native tissue-mimicking capacity of ECM constructs, Prasopthum et al. 3D printed a scaffold with ECM-like nanofibrous topography. MSCs cultured on the structures showed an improved cell adhesion, migration throughout the construct, and osteodifferentiation.[46]

2.1.4. Cell Proliferation. Following cell adhesion and morphology adaptation on a substrate, the rate of cell proliferation will also be affected by the nano- and micro-topographical surface structure. Surface roughness was examined in a study by creating substrates with different crystallinity ranges, followed by MC3T3 osteoblast-like cells culture. The study indicated that the cell proliferation rate was higher on surfaces with lower crystallinity and roughness on their surfaces.[47] In another study, surfaces with six different roughness values were made and were examined by culturing 3T3 murine fibroblasts on them.[48] Monitoring the cultured cells revealed that, although cell adhesion was higher on surfaces with $R_a \sim 50$ nm, the cell proliferation rate was higher on surfaces with lower to moderate roughness ($R_a \sim 40$ nm).[48]

Surface patterns, such as nanofibers (randomly or aligned oriented), have higher support for cell adhesion and cell proliferation rate.[49] Park et al. utilized TiO_2 nanotube's effects on cells by vertically orienting these tubes with different diameters as substrates for MSCs culture to explore surface patterning effects. After 3 days, it was shown that cell proliferation rate increased with decreasing nanotube diameter (highest cell count at 15 nm diameter and the lowest at 100 nm diameter).[50]

Investigating the cell behavior response to topography, MSCs were cultured on specialized poly(methyl methacrylate) PMMA films with nanoscale gratings.[51] Results from the culture indicated that the nanoscale grating topographies enhanced cell attachment, alignment, and proliferation rate on the surfaces.[51] A nanodesigned polystyrene with a structure of periodicity of 200−430 nm and a depth of 30−100 nm was created, and cultures of different mammalian cells on the surfaces showed that cell adhesion and proliferation rates were significantly improved by these nanostructures.[52] Macro- and meso-porosities in titania surfaces were examined with osteosarcoma cells culture. The specialized titania surfaces featuring macro- and meso-porosities reflected higher cell attachment, spreading, proliferation, and mineralization over smooth titania surfaces.[53] In microscales structures, Tanaka et al. designed linear substrates with widths of 80, 120, 160, and 200 μm used to culture different types of cells. On these substrates, control of cell adhesion and proliferation of nerve-like cells with widths of 10, 30, and 50 μm was possible.[54]

2.1.5. Cell Differentiation. As discussed, the structure's surface topographical cues could affect cell attachment, morphology, proliferation, and migration due to the effect on the cell integrin bindings and stress fibers. Furthermore, these changes can transfer to the nuclei through signaling pathways and cytoskeletons and regulate gene expression, which results in the changing of cell fate, especially in stem and progenitor cells. Several studies showed that ordered patterns stimulate stem cells to differentiate into neural-like cells. One such study investigated this by culturing neural stem cells on ordered nanofibers.[55] After 5 days, cells were not only aligned to the fibers but also expressed neuronal differentiation markers. On the other hand, the cells cultured on randomly distributed nanofibers or flat surfaces were not aligned and did not show neuronal differentiation.[55] In another study, hMSC cultured on nanograted structures (350 nm width) showed alignment to the ordered pattern with considerably upregulation neuronal markers.[56] Furthermore, ordered nanotopography generated by thermoresponsive nanofibers can direct MSC differentiation toward skeletal and cardiac muscle cells without the presence of any differentiation supplements.[57]

On the other hand, hMSCs could differentiate to other lineages by changing the topographic patterns. For example, hMSCs cultured on nanoscale disorder structures showed that cells were differentiated to osteoblast-like cells and produced bone minerals similar to control cells differentiated to osteoblasts in osteogenic media.[58] 3D topography design of the substrate at the micrometer and submicrometer levels can accelerate both the differentiation and maturation processes of induced pluripotent stem cells (iPSCs)-derived cardiomyocytes.[59] Moreover, it has been shown that cell shape can affect the lineage of their differentiation. Kilian et al., who cultured MSCs on pentagonal and rectangular shapes with different curvature and aspect ratios, respectively, explored this shape-dependent differentiation. Results from Kilian et al. revealed cells with distinct adipogenic or osteogenic profiles on different geometries.[60] Kilian et al. concluded that the geometries that caused actomyosin contraction also induced osteogenic differentiation.[60] Additionally, nanofibrous topographies on 3D printed polymeric scaffolds enhanced cell attachment and differentiation of hMSCs compared to smooth constructs.[46]

https://doi.org/10.1021/acsbiomaterials.1c00598
ACS Biomater. Sci. Eng. XXXX, XXX, XXX−XXX

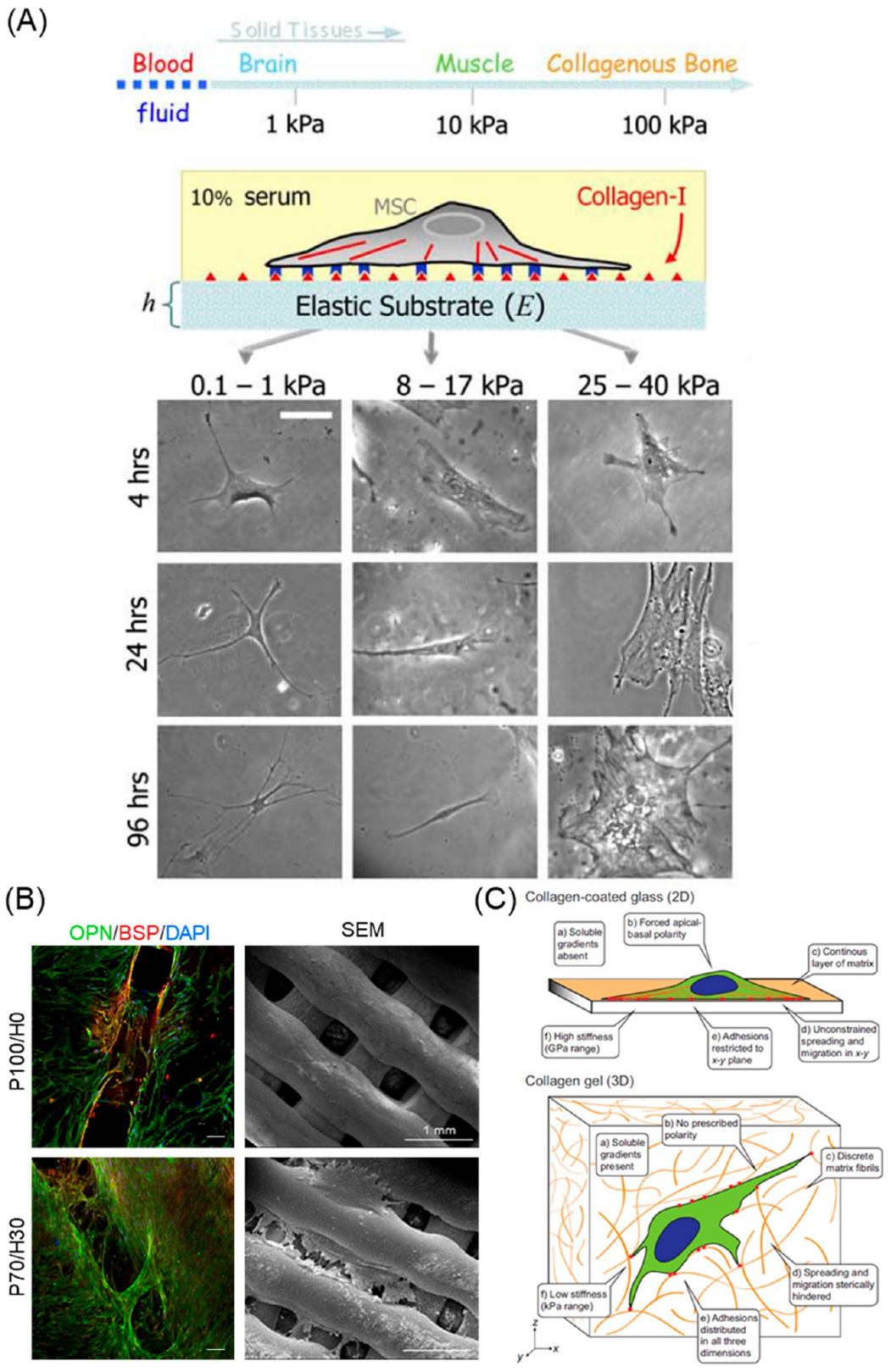

Figure 3. Cells react to the mechanical, composition, and geometrical properties of their environment. (A) Cultured MSCs on different elasticity ranges express different phenotypes that match cells in the tissues with the same native elasticities (scale bar is 20 mm). Reproduced with permission from ref 69. Copyright 2006, Elsevier. (B) Scaffold composition can change cell behavior. 3D printed structures with and without hydroxyapatite enhanced hMSCs attachment and differentiation to osteoblasts. Reproduced with permission from ref 15. Copyright 2020, Mary Ann Liebert, Inc. (C) Cells sense different cues in 2D and 3D environments. Reproduced with permission from ref 80. Copyright 2012, The Company of Biologists.

https://doi.org/10.1021/acsbiomaterials.1c00598
ACS Biomater. Sci. Eng. XXXX, XXX, XXX−XXX

While the majority of the results in literature have explored the cell response on continuous topographies, defects produced during the manufacturing process can locally change scaffold topography. This abrupt change can affect cellular organization and differentiation. The latter can be critical, as the formation of a random cell lineage across a large defective area can potentially compromise the overall biological function of the entire tissue.

2.2. Cell Mechanosensing (Mechanotransduction). The type of macromolecules and their concentration in the ECM varies by tissue, which defines the ranging mechanical properties from soft to hard tissues. Further, cells sense not only the substrate topography but also sense and respond to the stiffness of their environment.[61] Generally, cells prefer to grow on substrates with stiffness within their natural tissue stiffness range. However, when it comes to 2D culture, most cells prefer to adhere to stiffer surfaces. On the other hand, in 3D cultures, it would be easier for cells to anchor to a softer structure.[42] Importantly, changing the mechanical properties of the substrate can direct cell migration. For example, substrates with a gradient in their stiffness could direct cell migration from the softer to the stiffer zones of the substrate in 2D cultures.[42,62]

Furthermore, it has been shown that the increase in force on cancer cells is related to their migration and metastasis.[63] In addition, it is acknowledged that stem cells could be directed to differentiate to specific cell lineages by providing a substrate of a similar stiffness to the cell line's tissue. For example, low elastic moduli structures (<1 kPa) direct stem cell differentiation to neural cells, medium elastic moduli (10 kPa) direct differentiation to myogenic cells, and stiffer substrates (30−35 kPa) direct differentiation to osteogenic cells (Figure 3A).[64,65]

Pan et al. showed that different cross-linking degrees influence characteristics of the structure, such as the pore size, mechanical properties, water absorption, and cell behavior.[66] In many cases, with an increase in photo-cross-linking time, the hydrogel becomes stiffer, and cells cannot grow and expand sufficiently throughout the hydrogel.

Changes in the localized stiffness and mechanical properties of scaffolds can occur during various manufacturing processes. For example, in stereolithography-based printing, the nonuniform exposure of light can significantly change the stiffness throughout the scaffold. Similarly, during the extrusion of composite materials, the clogging or accumulation of materials in the nozzle area can result in a sudden change in the material composition and a nonuniformity in the mechanical stiffness of the scaffold. These can be translated into cellular responses that differ from the designed function.

2.3. Material Composition. Cell binding receptors have a high affinity to bind to macromolecules in their ECM, and these bindings affect cells as a result. Researchers in tissue engineering are trying to mimic cell bindings in their structures using different materials in their composites. For instance, integrin receptors have a high affinity for specific metal ions, such as Ca^{2+}, Mg^{2+}, and Mn^{2+}, increasing cell attachment. In Zhang et al.'s study, bone marrow stromal cells (BMSCs) were cultured on different magnesium/calcium phosphate cement composite ratios. The results proved that initial cell attachment increased and cells differentiated to osteoblasts due to integrin interaction with the composite component.[67]

While the materials in a composite affect cell adhesion, their distribution can affect cell spreading. The presence and dispersion of ECM proteins, such as collagen, laminin, elastin, and fibronectin, can significantly affect cell adhesion, spreading, and viability.[68] Moreover, materials with functional groups, such as $-NH_2$, $-SO_3H$, $-COOH$, epoxide, and $-OH$ can increase the cell adhesion and spread by increasing the wettability and protein adsorption of the surface of the composite.[69]

It has been well-known that the use of specific growth factors (e.g., bone morphogenetic protein (BMP)-2) in composite structures can induce cell recruitment and differentiation to a specific lineage (e.g., osteoblasts).[70] Furthermore, the presence of inorganic elements (e.g., calcium silicate and hydroxyapatite) in composites can direct the cell differentiation (e.g., osteoblasts) (Figure 3B).[71,72] As a result, changes in the composition of the scaffolds because the fabrication defects could affect the biological response. However, the impact of composition defects on tissue maturation is not well studied in the current literature.

2.4. Cells in Three-Dimensional Structures. As discussed earlier, the native cell environment in the body is a 3D multiscale construct, and understanding this complex environment is a growing need required for a better knowledge of cell responses in 3D environments (Figure 3C).[73] Many properties could be changed or added to 3D structures that could affect cells, producing different responses than 2D cultures. Since cells adhere to their substrate partially in 2D culture and with most of their surface area in 3D cultures, this substantiates that geometry significantly impacts cell response.

In one study, Ulrich et al. showed that by adding agarose to collagen, the elasticity of the gel increased and changed cell migration behavior from a mesenchymal manner to an amoeboid one.[74] Pore sizes and the degradation rate of the 3D structure can also affect cell adhesion and migration. For example, faster migration will happen in structures with a higher degradation rate. Furthermore, pore sizes equal to cell sizes (12 μm) expedite migration speed in comparison to pores smaller than cell sizes (7 μm) or larger than cells (17 μm).[75] Another study revealed that cubical pores in a 3D structure enhanced MSC differentiation into osteoblastic cells over alternatively cylindrical-shaped pores.[76] In this way, by choosing the proper pore size and shape when designing 3D implant structures, cell migration, infiltration, and differentiation can be improved.

3. EFFECT OF MATERIAL RHEOLOGICAL PROPERTIES ON PRINTING RESOLUTION AND QUALITY

Since the success of extrusion-based (bio)printing, whether it be cellular or acellular, relies on the rheology of (bio)inks, any deviation from what is considered "ideal behavior" may cause problems during extrusion/deposition. Achieving a balance between performance and maintenance of healthy cellular environments is instrumental in creating functional engineered tissues. Synthetic or natural biomaterials[77−80] may possess suitable rheology resulting in well-defined constructs but provide a suboptimal biological environment incapable of stimulating beneficial cell−substrate interactions.

On the other hand, ECM-mimicking biomaterials foster superior cell−substrate interactions but exhibit poor extrusion and depositional behavior in an unmodified state.[81−85] Therefore, the (bio)printing performance of (bio)inks is often improved by modifying their rheological properties. Some popular strategies to tailor the flow behavior of (bio)inks include; modifying the (bio)printing environment,[86] the use of innovative (bio)ink formulations,[87] altering cross-linking

https://doi.org/10.1021/acsbiomaterials.1c00598
ACS Biomater. Sci. Eng. XXXX, XXX, XXX−XXX

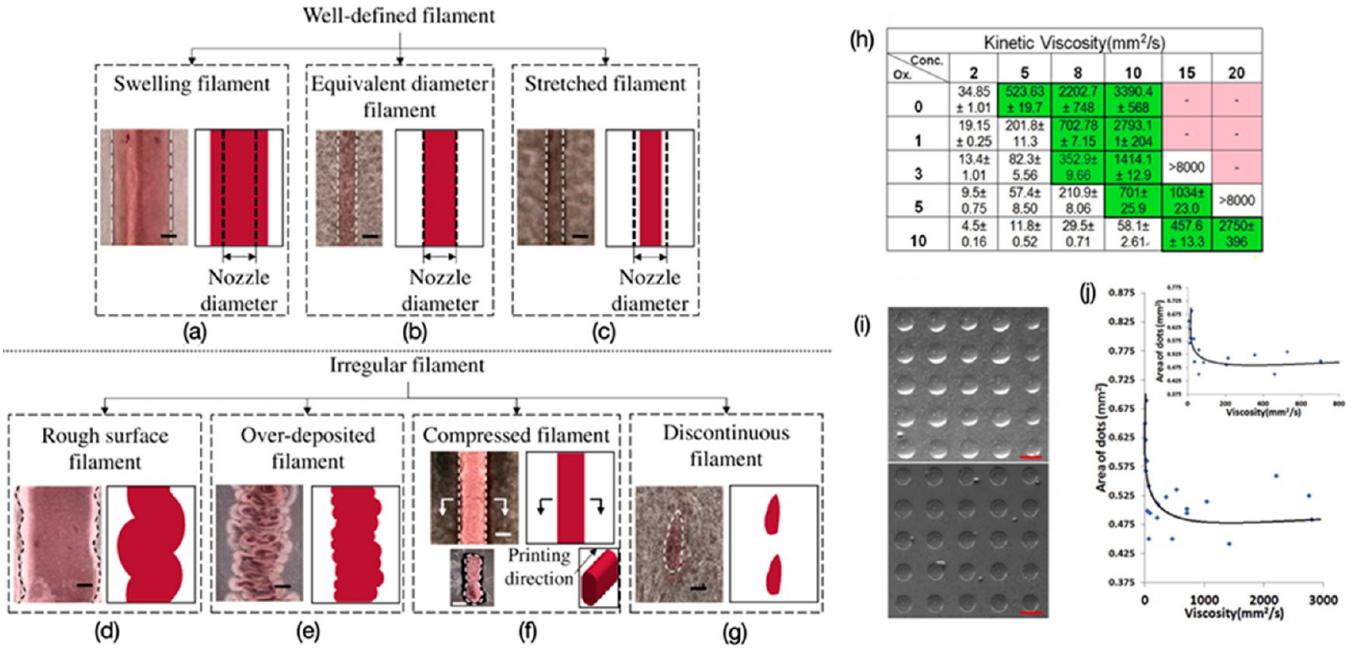

Figure 4. Same set of process parameters for a set of (bio)inks with distinct viscosities can lead to either regular or irregular filaments depending on the degree of match between flow properties and process parameters (Scale bars: 200 μm). Reproduced with permission from ref 102. Copyright 2017, Elsevier. (h–j) 5 × 5 dot arrays used for comparing resolutions of different alginate formulations. Reproduced with permission from ref 103. Copyright 2014, Elsevier. As the viscosity of the ink increased, the area of the printed dot decreased.

mechanisms,[88] and the use of sacrificial materials.[84,89] In this section, we describe the role of rheology in the generation of (bio)printing defects, along with strategies for modulating flow properties. Further reviews of biomaterial rheological properties can be found in the works of Malda et al.[90] and Ramesh et al.[13]

3.1. Viscosity. The nature of the polymeric network ultimately determines the viscosity of (bio)inks. Denser and heavier polymeric chains possess higher degrees of entanglement and offer resistance to deformational forces applied during extrusion.[91] As a result, viscous (bio)inks maintain their shapes longer and support the weight of subsequent layers during deposition. However, dense networks restrict migration of cells,[92] inhibit diffusion of nutrients and waste,[93,94] and require higher forces for extrusion.[95,96] Further, as solution viscosity rises, more shear stress will be exerted on encapsulated cells.[90] Therefore, balancing the benefits and limitations of high viscosity is essential. For instance, He et al. showed that the ideal viscosity for alginate/gelatin (bio)inks to achieve high resolution yet maintain cell function is in the range of 300−30 000 mPa·s.[97]

(Bio)inks are expected to exhibit shear-thinning (decreasing viscosity with increasing shear rate) and thixotropic behavior (increasing viscosity upon removing the shear rate) to facilitate extrusion and resist spreading.[98] Further, the viscosity of the (bio)inks determines the pressure and speed required for extrusion. While appropriate process parameters will lead to the creation of well-defined filaments, a mismatch between (bio)ink viscosity and process parameters can result in irregular filaments (Figure 4a–g).[99] Jia et al. used dots as functional units to compare the resolution of different ink formulations with different viscosities (Figure 4h).[100] Jia et al.'s printed dot array (5 × 5) showed examples of low and high printing resolution.[100] In Figure 4j, a plot dot areas versus viscosity shows the direct relationship between printability and viscosity of alginate samples.[100]

3.2. Yield Stress. The (bio)ink yield stress determines the minimum stress required to initiate flow. Yield stress plays a vital role in inhibiting phase separation of the (bio)ink and prevents undesirable leakage.[101] While high viscosity can delay the collapse of printed structures, high yield strength can prevent the merging of deposited strands.[90] Ribeiro et al. studied the role of yield stress in determining print resolution by comparing the different concentrations of poloxamer hydrogels. With these experiments, Ribeiro et al. showed that constructs printed with high yield stress (bio)inks were mechanically stable and yielded distinct features.[102] However, extremely high yield stress values can prevent the mixing of cells, and therefore, the yield stress needs to be tailored.

An emerging biofabrication approach, Freeform Reversible Embedding of Suspended Hydrogels (FRESH), allows soft biomaterials to be embedded in thermoreversible support baths at sizes ranging from a few millimeters to centimeters.[103] In FRESH bioprinting, the support bath needs to act like a Bingham plastic and behave as a rigid body at low shear stresses. This behavior is crucial in ensuring minimal resistance to a moving nozzle depositing biological materials. Through optimizing the yield stress of the support bath, complex structures mimicking the femur, branched arteries, embryonic hearts, and human brains have been printed. Using the FRESH approach, Lee et al. demonstrated the accurate printing of patient-specific cardiac ventricles with human cardiomyocytes.[104] Recently, Mirdamadi et al. demonstrated the large-scale 3D bioprinting of soft hydrogels using a compacted gelatin support bath material.[105] The high yield stress of the support bath used in FRESH holds (bio)inks in place until they are cured. Further, the bath must rapidly repair itself upon the removal of shear stress, returning to its former solid-like state, a trait known as thixotropy.[106]

https://doi.org/10.1021/acsbiomaterials.1c00598
ACS Biomater. Sci. Eng. XXXX, XXX, XXX−XXX

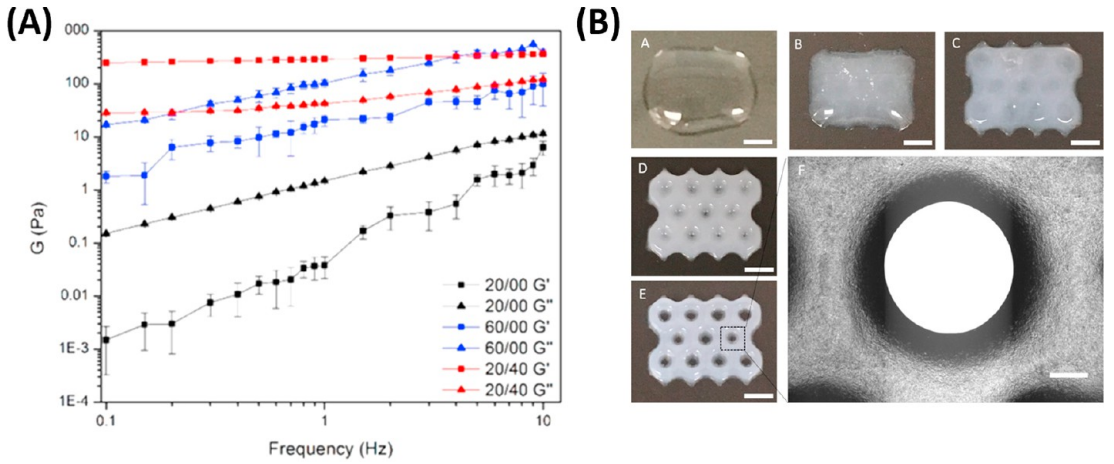

Figure 5. Effect of modulus on the (bio)printing performance of (bio)inks. (A, B) Wu et al. demonstrated that the storage modulus of the (bio)inks determined the pore-definition in a printed scaffold. In general, (bio)inks with higher storage modulus values produced liver-mimetic 3D honeycomb structures with the highest print accuracy. Reproduced with permission from ref 111. Copyright 2018, Elsevier.

3.3. Dynamic Modulus. The (bio)printing behavior of (bio)inks is affected by dynamic modulus, which is made of two components: (a) storage and (b) loss modulus. Storage modulus is indicative of a material's ability to store energy, and loss modulus is indicative of the tendency to dissipate energy. Extrusion involves applying low and high-frequency deformations, so changes in the moduli during the application of force can help identify suitable (bio)printing regimes.

(Bio)inks exhibit gel-like behavior when the storage modulus exceeds the loss modulus and solution-like behavior when the loss modulus is higher than the storage modulus. The loss factor, a ratio of loss to storage modulus, is a valuable predictor of printability and should be closely monitored to control extrusion and gelation.[107] Further, the gelation status of a (bio)ink at the time of extrusion also impacts the defect occurrence.

For instance, when undergelled (loss modulus > storage modulus), (bio)inks form temporary strands that merge with adjacent strands immediately after their deposition and result in poorly defined pores. In contrast, overgelled (storage > loss) (bio)inks yield wrinkled and fractured filaments and cause material discontinuity, which ultimately results in inferior feature definition and poor mechanical performance. Gao et al. demonstrated that the quality of printed constructs depends on the ratio of loss to storage moduli.[107] Ratios between 0.25 to 0.45 led to consistent, well-defined constructs when printing a combination of gelatin and alginate. The moduli of (bio)inks are tailored by varying the polymer concentration during process optimization (Figure 5A and B).[85,108,109]

3.4. Shear Stress. Extrusion involves the application of force to facilitate the flow of (bio)inks through nozzles. During extrusion, the (bio)ink is sheared against the syringe and the nozzle walls, which may lead to impaired cellular function.[110,111] The magnitude of shear stress experienced by the (bio)ink is directly proportional to viscosity and inversely proportional to the nozzle diameter.[112,113] High viscosity (bio)inks (bio)printed with small nozzles give rise to high-quality structures without dimensional defects. However, the application of high shear to initiate and maintain the flow of these (bio)inks might compromise cell viability. As a result, the length of the printing nozzle needs to be diligently evaluated to minimize cell death during extrusion.[114] Maximum shear stress in the nozzle has an exponential relationship with cell viability.[115] Among nozzles of different geometries, conical nozzles show only one location of high shear at the exit of the orifice compared to straight tip nozzles, which have high shear throughout the entire nozzle.[116] Recently, Ho et al. showed that shear stress generated by EBB could be beneficially exploited to perform in situ transfection.[117] Ho et al. demonstrated fibroblasts could be reprogrammed into neural crest-stem like cells by maintaining an average shear stress close to 190 Pa.[117] The result is hypothesized to be due to shear stress from the printing process causing a transient membrane permeability required for transfection.[117] The approach holds promise for drug screening and is an example of benefiting from the inevitable presence of shear stresses during extrusion printing. With increasing awareness about the detrimental effects of shear stresses on cellular function, research efforts focusing on tailoring rheological performance and predicting cellular response to extrusion forces have become integral to advancing (bio)printing research.

4. MODULATING RHEOLOGY OF (BIO)INKS

Tailoring the flow behavior of (bio)inks is of particular interest to tissue engineers. These efforts are geared toward achieving two objectives: (a) creating defect-free (bio)printed constructs and (b) maintaining a suitable biological environment for cells. The benefits of modulation strategies can only be fully assessed after analyzing the performance of (bio)inks on both fronts. Here, we provide an overview and discuss the effectiveness of the strategies proposed for altering the flow behavior of (bio)inks used in EBB. For further information on modulating hydrogel rheology, the review of Lee et al. discusses the topic in much greater depth.[118] In addition, a summary table of the material design components discussed in this section can be seen in Table 2.

4.1. Modifying Concentration. The most common route to modulate the (bio)ink viscosity is to adjust polymer concentration. Increasing the polymer concentration can discourage droplet formation during extrusion and aid in the formation of filaments.[90] Bertassoni et al. demonstrated that higher concentrations (7−15%) of gelatin methacrylate (GelMA) provide better printability than lower GelMA concentrations.[119] Lower concentrations (<7%) of the (bio)-inks were not easily (bio)printed and failed to generate well-defined pores and uniform struts.

https://doi.org/10.1021/acsbiomaterials.1c00598
ACS Biomater. Sci. Eng. XXXX, XXX, XXX−XXX

Table 2. Example Material Designs for Mechanical or Rheological Properties in Bio-AM

research group	material design	rheological and mechanical property	cell/tissue type	research highlights	ref
Schuurman et al. (2011)	polycaprolactone (PCL)/sodium alginate (SA)	2% SA – low viscosity, poor control over porosity, poor mechanical properties PCL – improved stiffness PCL-SA – Young's modulus (6 MPa) six times greater than SA	C20A4 cells for musculoskeletal regeneration	successfully used a hybrid printing approach for tailoring the mechanical properties of printed scaffolds	136
Zhang et al. (2017)	polycaprolactone (PCL)/polylactide-co-caprolactone (50:50); fibrin, gelatin, and hyaluronic acid	PCL – high stiffness (high tensile stress, low elasticity)	bladder urothelial cells (UCs) and smooth muscle cells (SMCs) for urethral regeneration	spiral designs mimicked the Young's modulus, strain at break, and tensile stress of the native urethra	137
Ma et al. (2018)	decellularized extracellular matrix (dECM)/Gelatin methacryloyl (GelMA)	dECM – tuned to mirror the native environment	HepG2 cells for cirrhotic liver models	cross-linked GelMA for different times to achieve proportionally different mechanical properties. HepG2 cells grown on stiffer scaffolds showed higher levels of apoptosis and CASP8, indicating the relevance of the tissue model	85
Kundu et al. (2015)	polycaprolactone (PCL)/sodium alginate (SA)	PCL – superior mechanical properties SA – low viscosity, ill-defined structures	chondrocytes, TGFβ	3D architecture and mechanical properties of PCL were combined with the bioactive SA to create hybrid scaffolds	138
Kolesky et al. (2016)	gelatin, fibrinogen cross-linked by enzymatic thrombin and transglutaminase (TG)	TG – enzymatic cross-linker gives mechanical and thermal stability needed for long-term perfusion	HMSCs, human neonatal dermal fibroblasts, HUVECs	3D vascularized tissues were perfused with growth factors for >6 weeks to differentiate MSCs into osteogenic lineage	139
He et al. (2016)	sodium alginate (SA)/gelatin	SA – poor pore retention gelatin – improves mechanical strength, provides structural integrity until SA is cross-linked	L929 mouse fibroblasts	hybrid hydrogel was used to print cell-laden structures, and the approach controls cross-linking without altering biocompatibility	97
Tan et al. (2015)	sodium alginate (SA)	SA – easily modifiable by changing cross-linking chemistry	acellular	xanthan gum was used as an additive, improving the structural stability and allowing the printing of vertical tubular structures	140
Khalil et al. (2009)	sodium alginate (SA)	SA – between 1.5 and 2% SA yielded sufficient viscosity for printing	endothelial cells	window of allowable shear stress values within which the viability of cells does not change was identified	141
Kang et al. (2016)	polycaprolactone (PCL)/(gelatin, fibrinogen, hyaluronic acid, glycerol)	PCL – rigid structure	human AFSCs, chondrocytes, mouse C2C12 myoblasts	patterning PCL in hydrogel scaffolds offered mechanical strength to the scaffold	142
Rhee et al. (2016)	collagen	capable of supporting load-bearing applications when used in high concentrations	primary fibrochondrocytes	heterogeneous 3D-printed constructs were generated with discrete domains possessing distinct mechanical properties	143
Lee et al. (2013)	collagen	high viscosity collagen can represent the dominant structures of skin tissue	fibroblasts, keratinocytes	constructed 3D tissue with dermal and epidermal compartments in a single structure	144
Hutmacher et al. (2001)	polycaprolactone (PCL)	PCL – can be applied to soft- and hard-tissue applications	acellular	by altering thermoplastic strand orientation and spacing, different mechanical properties were produced	145
Bertassoni et al. (2014)	gelatin methacryloyl (GelMA)	GelMA – elastic moduli can be tailored by changing exposure time to UV light	HepG2, fibroblast cells	printing prepolymerized hydrogel fibers demonstrated the relationship between debonding and applied load	119
Yin et al. (2018)	gelatin/gelatin methacryloyl	possess sufficient yield strength in high concentrations	BMSCs	flexible cross-linking mode for stabilizing the mechanical integrity of bioprinted structures	120
Jia et al. (2016)	gelatin methacryloyl/sodium alginate/polyethylene glycol-tetra-acrylate (PEGTA)	PEGTA – enhanced cross-linking, high mechanical strength	HUVECs, MSCs	specialized coaxial nozzles were used to print perfusable constructs	86
Skardal et al. (2010)	hyaluronic acid/tetrahedral polyethylene glycol tetracrylates (TetraPAC)-cross-linked synthetic extracellular matrices (sECMs)	polyethylene glycol polymers – chain lengths are easily controlled to tune mechanical properties	murine fibroblasts (NIH 3T3), human hepatoma (HepG2 C3A)	tetraPAC-cross-linked sECMs outperformed PEGDA-cross-linked hydrogels with the same composition	146
Muller et al. (2017)	sodium alginate/nanocellulose	nanocellulose – provides shear thinning behavior	bovine chondrocytes	straight nozzles displayed two areas of high shear, while the cylindrical nozzles had only one high shear area	116
Shin et al. (2017)	cellulose nanofibril (CNFs)/gelatin methacryloyl (GelMA)	CNFs – imparts excellent physical and mechanical properties	NH3T3 cells	milled CNFs with low GelMA concentrations had printable viscosity and favorable mechanical strength	123

https://doi.org/10.1021/acsbiomaterials.1c00598
ACS Biomater. Sci. Eng. XXXX, XXX, XXX−XXX

Table 2. continued

research group	material design	rheological and mechanical property	cell/tissue type	research highlights	ref
Zhao et al. (2015)	sodium alginate (SA)/gelatin	SA – poor pore retention gelatin – improves mechanical strength, provides structural integrity until SA is cross-linked	A459 cells	storage modulus (<382 Pa) should be achieved to get a survival rate of 90% Determined rheological properties to be the sole influence on cell survival rate	147
Lee et al. (2018)	collagen/tannic acid (TA)	collagen – tunable mechanical and rheological properties	MC3T3 cells	compared to the cell-laden collagen scaffold without TA cross-linking, the scaffold with TA cross-linking was significantly enhanced in mechanical properties, while reasonable cellular activities were observed	148
Wilson et al. (2017)	K-carrageenan (kCA)/nanosilicate	kCA – shear thinning behavior	MC3T3-E1 cells	bioinks possessed shear thinning characteristics and cross-linked under physiological temperature	122
Shim et al. (2012)	polycaprolactone (PCL)/sodium alginate (SA)	PCL – superior mechanical properties SA – easy to handle	osteoblasts, chondrocytes	MtoBS enabled the dispensing of biomaterials to develop scaffolds for the regeneration of heterogeneous tissues	149
Blaeser et al. (2016)	sodium alginate (SA)	SA – shear-thinning behavior	hMSCs	short-term exposure to shear stress can have a long-term impact on cell behavior	110
Li et al. (2015)	polypeptide DNA + DNA linker	DNA-hydrogels—nonswelling/shrinking; permeable to nutrients	AtT-20 cells	demonstrated the rapid formation of a supramolecular polypeptide-DNA hydrogel. The printed gels possessed high mechanical strength and nonswelling properties	150
Miranda et al. (2008)	tricalcium phosphate (TCP) and hydroxyapatite (HAp)	TCP/HAp – brittle materials, highly relevant compositional similarity to the bone	NA	robocasting of TCP and HAp inks. Immersion in simulated body fluid was used to modulate the mechanical properties of HAp scaffolds	151
Senatov et al. (2016)	polylactic acid (PLA)/hydroxyapatite (HAp)	PLA – shape memory effect for self-fitting	NA	PLA structures with a bioactive component HAp showed shape memory properties	152
Pfister et al. (2004)	polyurethane (PU)	PU – advantageous mechanical properties and tailorable molecular structure	NA	compared scaffolds fabricated using 3D printing versus 3D bioplotting	153
Luo et al. (2017)	Sodium alginate (SA)/polyvinyl alcohol (PVA)	SA – prone to diffusion when used in low concentrations	BSA and BMP-2	macro-pores were controlled by 3D printing, while micropores were controlled by PVA concentration	154
Wu et al. (2016)	collagen/sodium alginate (SA)/gelatin	SA – maintains shapes and hardens upon cross-linking	human corneal epithelial cells	with the molar ratio of sodium citrate/SA, construct degradation time can be controlled	155
Temple et al. (2014)	polycaprolactone (PCL)	PCL – suitable for load-bearing applications because of superior mechanical properties	acellular printing	infill density of the scaffolds was varied to identify the best configuration to maximize cell growth and the uniformity of distribution	156
Lee et al. (2016)	polycaprolactone (PCL)/collagen	PCL – offers structural integrity	hepatocytes, HUVEC, lung fibroblasts	PCL framework protected the hydrogel from premature degradation and facilitated urea and albumin synthesis	157
Park et al. (2017)	low and high molecular weight (MW) sodium alginate	needs modification to offer good mechanical stability	NIH 3T3 fibroblasts	combination of high and low MW alginate in a ratio of 2:1 offers favorable printability and cell environment	135
Serra et al. (2013)	polylactic acid/calcium phosphate glass	Mechanical integrity and tailorable degradation	acellular	mechanical strength of orthogonal layer configuration was three times greater than the displaced double-layer design	158
Jakus et al. (2016)	polycaprolactone/polylactic acid	hyperelasticity	acellular	demonstrated high levels of elasticity capable of undergoing greater than 35% strain without failure	159
Bakarich et al. (2015)	poly(*N*-isopropylacrylamide) (PNIPAAm)/sodium alginate (SA)	PNIPAAm/SA – mechanically robust	acellular	demonstrated excellent printability, restricted swelling, and improved mechanical performance	160
Wilson et al. (2017)	Kappa-carrageenan (kCA)/Nanosilicate	kCa – viscosity enhancer	acellular	addition of kCA improved the shear-thinning and shape-retention property and resulted in the printing of highly structured constructs	122

https://doi.org/10.1021/acsbiomaterials.1c00598
ACS Biomater. Sci. Eng. XXXX, XXX, XXX−XXX

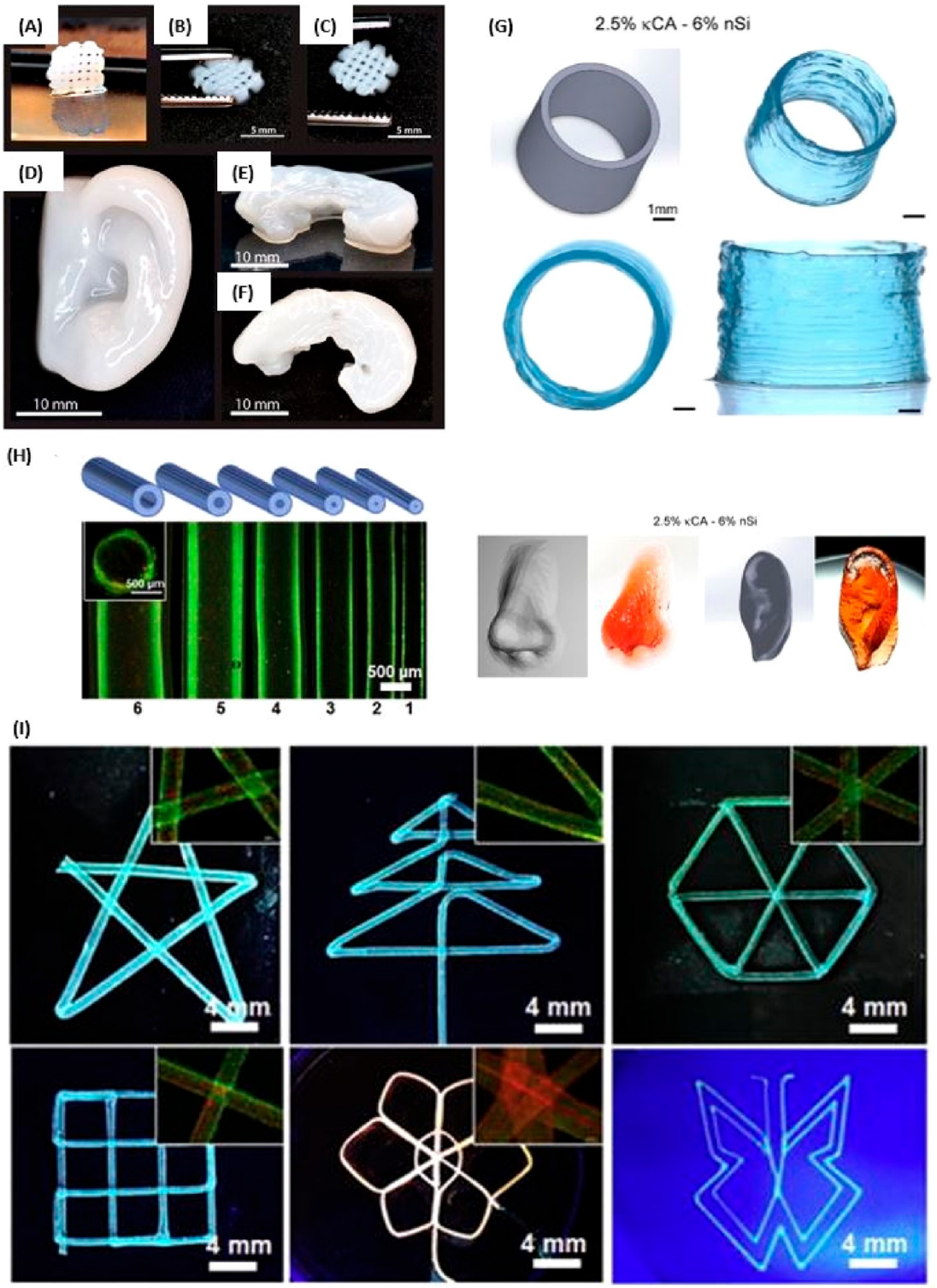

Figure 6. Additives are commonly added to (bio)inks to improve (bio)printing performance. (A−F) Markstedt et al. used nanocellulose as an additive to improve the viscosity and shear-thinning behavior of low concentration alginate (bio)inks to produce high definitions structures cartilage regeneration. Reproduced with permission from ref 130. Copyright 2015, ACS Publications. (G) Wilson et al. added nanosilicates to kappa-carrageenan (bio)inks to produce complex structures. With increasing levels of nanosilicates, the viscosity recovery behavior of the (bio)inks was improved. Reproduced with permission from ref 125. Copyright 2017, ACS Publications. (H−I) Addition of PEGTA allowed for the creation of flawless perfusable structures. Reproduced with permission from ref 89. Copyright 2016, Elsevier.

Yin et al. showed that the concentration of gelatin and GelMA in the hybrid hydrogels created the difference between inconsistent, unprintable, and printable hydrogels.[120] Lower concentrations of gelatin (0−2%) and GelMA (0−10%) showed signs of longitudinal instability at the nozzle outlet and caused spindle-shaped filaments. The high concentration (bio)inks containing gelatin (6−10%) and GelMA (>20%) were viscous and formed wrinkled filaments. An ideal

https://doi.org/10.1021/acsbiomaterials.1c00598
ACS Biomater. Sci. Eng. XXXX, XXX, XXX−XXX

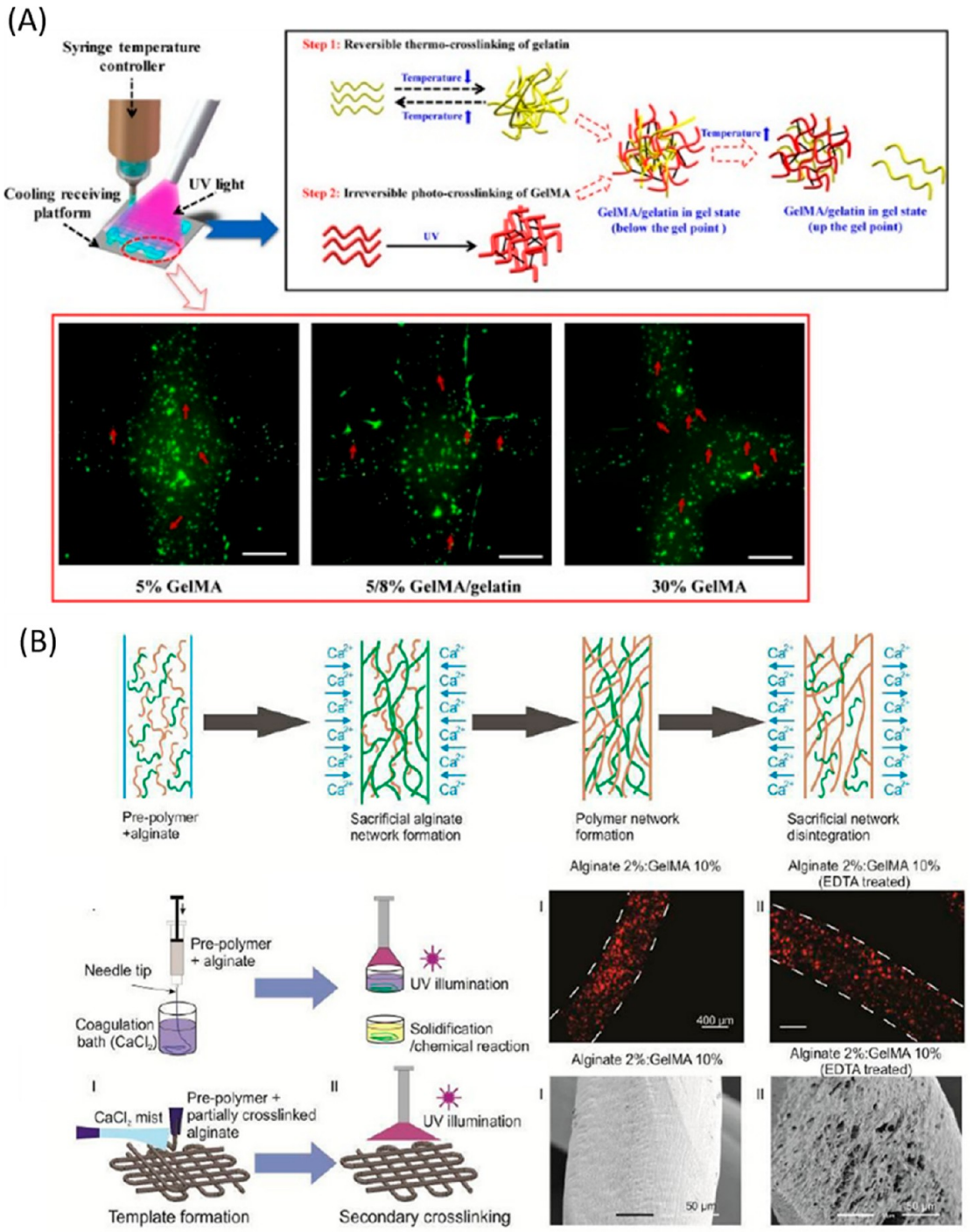

Figure 7. Dual cross-linking strategies are effective at providing mechanical stability during (bio)printing. (A) Yin et al. developed the strategy for 3D bioprinting of low-concentration cell-laden GelMA (bio)inks by adding gelatin. The 5% GelMA (bio)inks with gelatin were successfully extruded into stable 3D constructs using a two-step thermal-/photo-cross-linking strategy. Reproduced with permission from ref 123. Copyright 2018, ACS Publications. (B) Tamayol et al. presented an innovative approach for making sacrificial polymer templates that can be used for creating complex 3D constructs for various applications. Reproduced with permission from ref 87. Copyright 2015, John Wiley & Sons, Ltd.

concentration of 5% GelMA and 8% gelatin was chosen as it yielded structures with dimensions close to the target and provided interconnected grid structures without internal pore collapse. Although increasing the polymer concentration can provide stable filaments, an unchecked increase in concentration can negatively affect the cellular environment by inhibiting oxygen and nutrient diffusion. Therefore, the use of high molecular weight polymers in moderate concentrations has been cited as an optimal approach.[121]

4.2. Use of Additives. A popular approach to tailor the viscosity-related behavior of (bio)inks is to use additives, such as nanocellulose, carrageenan, hyaluronic acid, gellan gum, etc.[118,122−125] Tan et al. improved the viscosity of low-concentration alginate hydrogel by including xanthan gum.[126] The formulation's apparent viscosity increased from 30 Pa·s at

https://doi.org/10.1021/acsbiomaterials.1c00598
ACS Biomater. Sci. Eng. XXXX, XXX, XXX−XXX

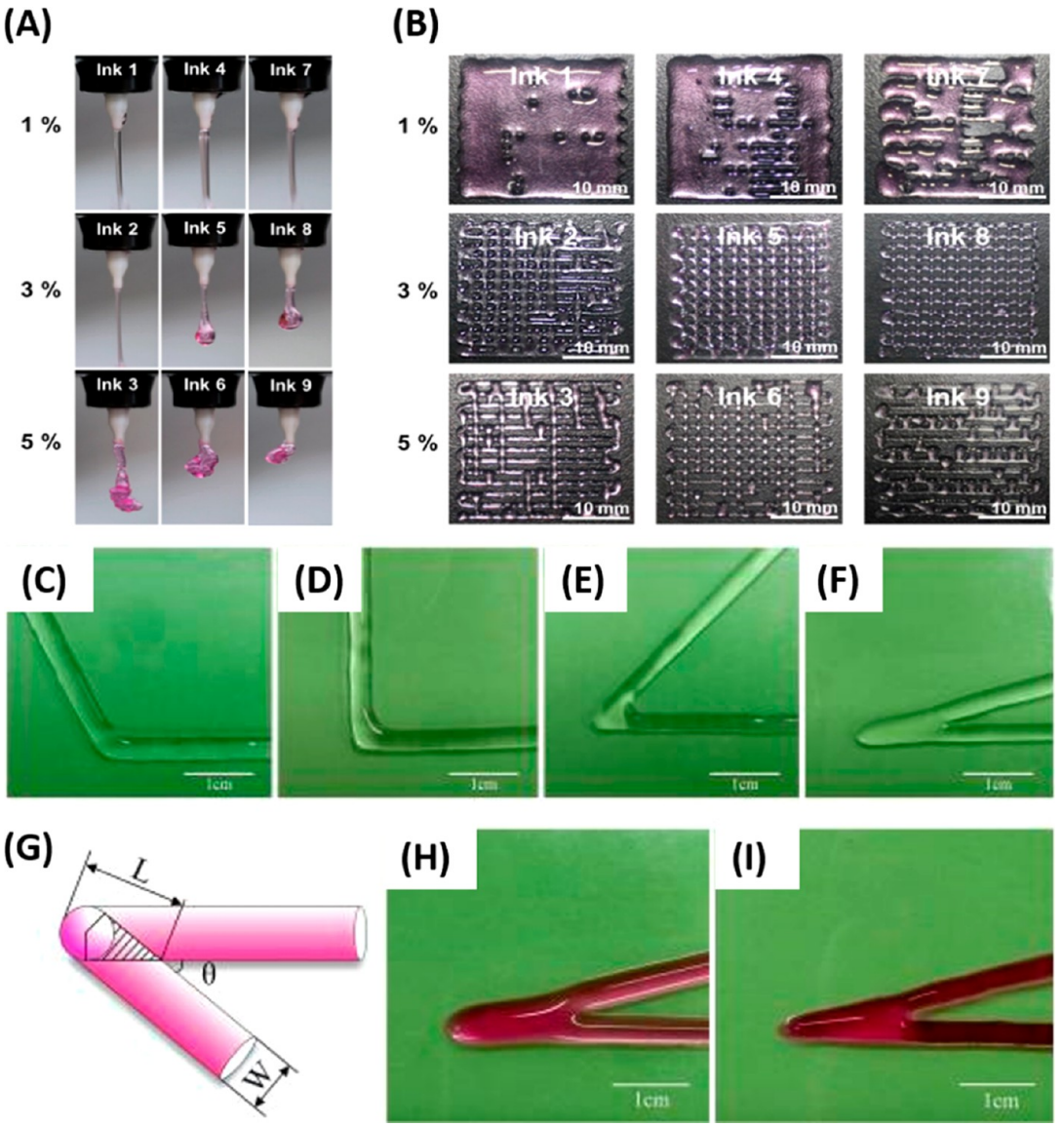

Figure 8. Blending of different hydrogels can result in printable ink with suitable rheological behavior. (A, B) Park et al. demonstrated that the molecular weight of the blended hydrogels could influence printing performance. Low molecular weight gels possess low viscosity and cause fusion defects, while high molecular weight gels possess high viscosity and cause difficulties during extrusion. Reproduced with permission from ref 138. Copyright 2017, Elsevier. Other than attaining viscosity in the ideal range, He et al. (C–I) showed that two other strategies could avoid nonuniform extrusion. The first method is avoiding the sharp angle in the printing path generation. However, the sharp line could not be avoided when printing sharp structures. The second method is reducing the extrusion rate in this area from the standard extrusion to halved extrusion. Reproduced with permission from ref 100. Copyright 2016, Elsevier.

1% additive to greater than 50 Pa·s at 3%. At lower concentrations of xanthan gum, the tubular structures became increasingly out-of-roundness because of inadequate viscosity and became unstable due to insufficient extrusion at higher concentrations. At 2% xanthan gum, the hydrogel yielded tubular constructs that matched the predesigned roundness.

Of the multitude of additives reported to impart shear-thinning behavior, nanofibrillated cellulose (NFC) and Laponite have been widely used because of their remarkable viscosity-enhancing and shape-retention properties even at low concentrations (Figure 6A–G).[122,127–129] In a study involving alginate-NFC (bio)inks, Muller et al. reported the dramatic improvement in printability of low-concentration alginate without altering its cross-linking performance.[116] The concentration of additives must be tailored to not interfere with cross-linking and must not increase the density of the polymeric network to avoid hindering oxygen diffusion. In another study, 2% poly(ethylene glycol)-tetra-acrylate (PEGTA) was used as an additive to alginate/GelMA solutions. The improved printability was likely due to the branching of the PEG molecules, which provided the mechanical stability required to generate flaw-free perfusable constructs with hollow interiors (Figure 6H–I).[86]

4.3. Crosslinking Strategies. Thixotropic (bio)inks recover their viscosity after extrusion but need further stabilization, which is achieved by cross-linking the construct. Exposure to a chemical cross-linker,[130] changes in temperature,[131] or ultraviolet (UV) light are some of the well-tested cross-linking strategies in biofabrication.[132] Nevertheless, none of these strategies are instantaneous, requiring the completion of a chemical reaction, which provides enough time for defect propagation (i.e., the collapse of tubular structures, strand

https://doi.org/10.1021/acsbiomaterials.1c00598
ACS Biomater. Sci. Eng. XXXX, XXX, XXX–XXX

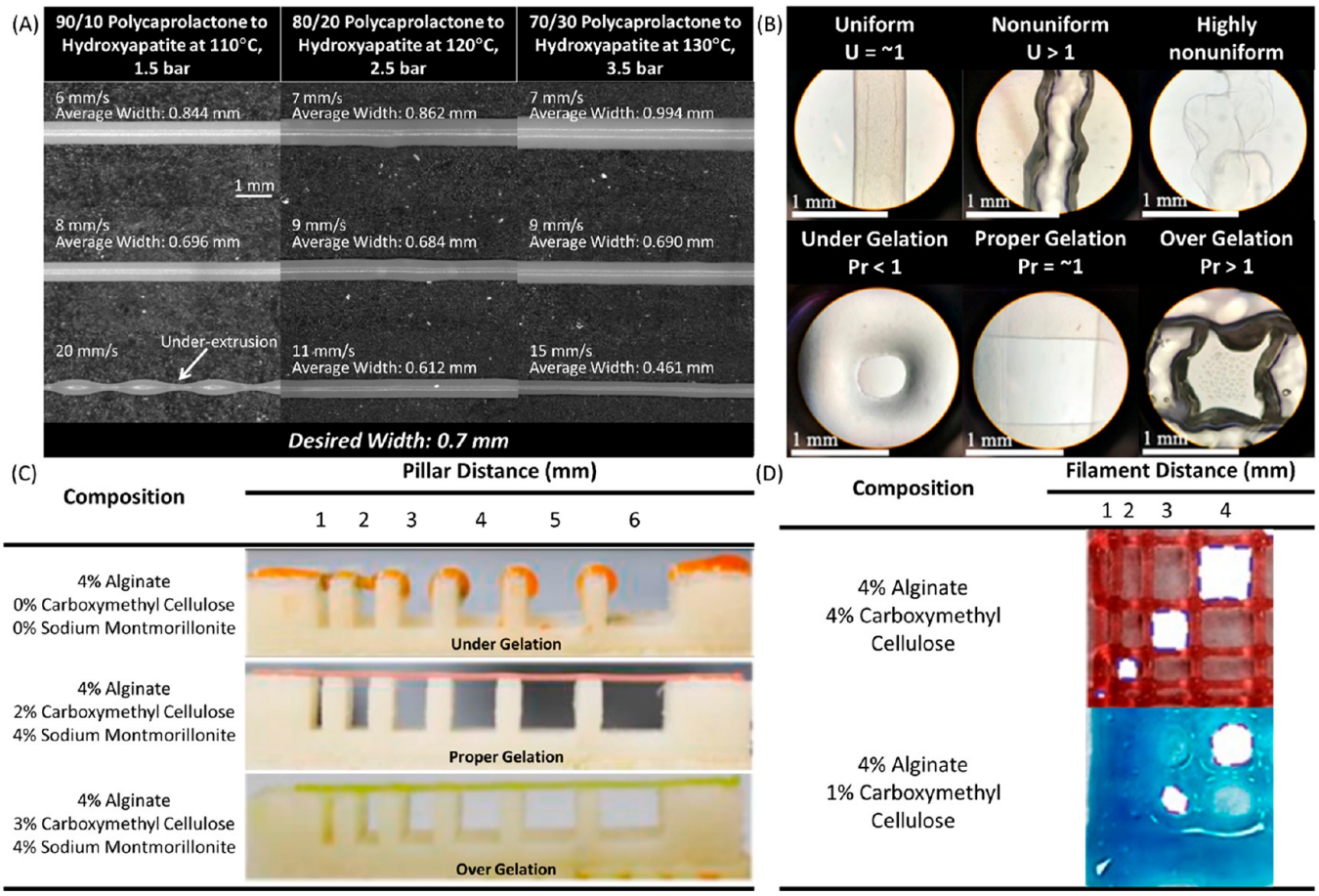

Figure 9. Print defects in biological additive manufacturing. (A) Gerdes et al. demonstrated the effects of material composition and print parameters (such as temperature, extrusion pressure, and print velocity) on strand width. Reproduced with permission from ref 15. Copyright 2020, Mary Ann Liebert, Inc. (B) Soltan et al. evaluated strand and pore geometry defects in alginate dialdehyde/gelatin hydrogels due to gelation. Reproduced with permission from ref 16. Copyright 2019, American Chemical Society. (C) Habib et al. printed on a specialized mount (consisting of set overhang distances) with alginate/carboxymethyl cellulose/sodium montmorillonite hydrogels, showing material composition's role in strand collapse. Reproduced with permission from ref 18. Copyright 2018, Elsevier. (D) Habib et al. illustrated strand fusion testing in alginate/carboxymethyl cellulose composites (where the dotted boundary denotes the edge of a pore) by printing a gradient of interfilament distances. Reproduced with permission from ref 17. Copyright 2018, Multidisciplinary Digital Publishing Institute.

fusion, curving of edges, etc.). In that regard, there has been an increase in innovative cross-linking strategies capable of balancing quality and cellular health.

For instance, Yin et al. employed two-step gelation to bioprint high-fidelity gelatin/GelMA constructs containing bone marrow stem cells (BMSCs) (Figure 7A).[120] The inclusion of gelatin allowed the thermal cross-linking of the printed structure, which helped with the mechanical stability of the extruded (bio)ink until the photopolymerization reaction was completed. The dual cross-linking strategy allowed the utilization of low-concentration GelMA solutions, which would otherwise possess poor processability. In a contrasting approach, Ouyang et al. developed a hyaluronic acid (HA)-based hydrogel that was first cross-linked using UV light then thermally stabilized at 37 °C.[133] The cross-linking strategy allowed the printing of HA-based systems without other additives or hydrogels for improved mechanical stability. Coaxial printing allows the simultaneous printing of a hydrogel and a cross-linker solution to print low viscosity solutions with improved stability.[80,86]

In another study, Tamayol et al. demonstrated a robust approach using alginate as a sacrificial polymer template (Figure 7B).[84] The alginate-based sacrificial template could be used to fabricate fibers from many bioactive hydrogels (gelatin, GelMA, poly(vinyl alcohol), agarose, poly((ethylene glycol) diacrylate), and Tamayol et al. further demonstrated the wet spinning and direct writing of the sacrificial network. The entrapped polymer within the alginate template was subsequently cross-linked and formed an independent polymeric network. The use of such a sacrificial template enabled the creation of complex, multimaterial frameworks for tissue regeneration applications.

4.4. Multicomponent Hydrogels. The rheology of hydrogels is modified by blending them with other hydrogels. Multicomponent formulations benefit from the synergistic effects of mixing chemically, morphologically, and functionally different solutions.[134] For instance, Park et al. investigated the rheology of combinations of low (1.43×10^5 g/mol) and high (3.5×10^5 g/mol) molecular weight (MW) alginate gels.[135] These alginate gels demonstrated a strong correlation between MW and the flow behavior of the hydrogels. The low MW alginate solutions flowed more readily, while high MW solutions possessed superior shape-retention. Low MW alginate-containing (bio)inks possessed insufficient viscoelastic properties resulting in merging defects. On the other hand, (bio)inks containing increased amounts of high MW alginate

https://doi.org/10.1021/acsbiomaterials.1c00598
ACS Biomater. Sci. Eng. XXXX, XXX, XXX−XXX

offered little control over extrusion and provided poor feature definition. Park et al. also formulated an optimized (bio)ink consisting of 3% (w/v) alginate (Ink 2) (1:2 low:high MW alginate), which provided excellent flow behavior and printability (Figure 8A and B).[135]

In another study, hybrid hydrogels consisting of alginate and gelatin were created.[97] To formulate a gel with a desirable viscosity of 300−30 000 cps, that does not require high pressures and has good shape retention; gel viscosities (at 37 °C) from a series of alginate−gelatin (alginate, 1−5% (w/v); gelatin, 2−10% (w/v)) mixtures were compared. A combination of 2.5% alginate and 8% gelatin was chosen for bioprinting scaffolds with fibroblasts. He et al. also showed that, despite having suitable viscosity, the extrusion rate at the corners had to be reduced to half of the original rate to achieve defect-free sharp corners (Figure 8C−I).[97]

5. DEFECTS CAUSED BY SUBOPTIMAL PRINTING PARAMETERS

As discussed above, scaffold fabrication is an intricate balancing act between favorable cellular response and suitable material properties. Further complicating this balance is the (bio)-printing process itself, which introduces numerous process parameters that need proper management. These process parameters (such as pressure, temperature, speed, strand spacing, etc.) are intimately tied to construct quality, and incorrect settings can lead to severe print defects that could influence the cell response, the mechanical properties of the scaffold, or both.

As a result, a material's process parameters typically undergo optimization to minimize the occurrence of strand diameter imperfections, unwanted strand fusion, strand collapse, and pore geometry defects. While material composition, cross-linking degree, surface topography, and cell distribution are important parameters that can deviate from the intended design, tools for detecting their imperfections have not been researched. Therefore, in the following section, geometrical defects will be examined regarding their propagation, evaluation, and prevention.

5.1. Imperfections in Homogeneity of Strand Diameter. In 3D (bio)printing, process resolution is of high importance, as it indicates the smallest feature size the (bio)printing setup (printer type, material, print parameters, etc.) is capable of fabricating. In EBB, the resolution is directly tied to strand diameter, and an increase in needle diameter is considered a decrease in print resolution.[164] However, strand diameter is also influenced by process parameters such as pressure, temperature, and print speed.[72] Therefore, improper strand diameter is the symptom of improper process conditions, leading to strands larger or smaller than the targeted diameter or discontinuous line fragments. Furthermore, pressure is a very important consideration among the process conditions, as a material's flow rate is proportional to the applied pressure.[161−165]

Further, the applied pressure must overcome the yield threshold of the print material for consistent extrusion; otherwise, discontinuous strands will be created.[97,161−163] Print speed is also a significant influencer of strand diameter, where strand diameter is inversely related to print speed (see Figure 9A).[72,164] The impact of print speed is also dependent on the pressure being used, as changes in print speed have a more pronounced effect in high-pressure applications.[72,164] Further, if the print speed is too high for the current flow rate, the generation of discontinuous strands is possible.[72,164] Finally, the cross-linking degree can influence strand diameter, as under-cross-linked material is susceptible to spreading.[162,163] While strand diameter is an essential indicator of strand quality, it is only half of the picture. To fully assess strand quality, it is also essential to consider a strand's uniformity, or how closely its path aligns with the theoretical deposition.

Evaluation of strand diameter comes in the form of postprint microscopy or optical imaging followed by image analysis.[161−165] Because these measurements are done through postprint processing, errors will only be evident after the print has been concluded, potentially resulting in a loss of time and resources. In strand uniformity detection, strand length is compared to its theoretical length through equation 2.[161] Uniform strands ($U = 1$) feature approximate lengths to the theoretical model, and nonuniform strands ($U > 1$) feature significantly meandering paths, deviating from the ideal strand length (see Figure 9B).[161]

The prevention of strand diameter defects is primarily done by optimizing the process parameters for a specific material.[72,97,164,166] For example, using a set temperature, pressure can be held constant while print velocity is varied or vice versa, and the strand diameters can be observed (see Figure 9A).[72,164,166] In thermoplastic or materials without cell encapsulation, the most desirable parameter arrangements yield both high resolution and consistency. In contrast, cell encapsulated hydrogels must be optimized to maximize print resolution and minimize shear stress during extrusion to reduce the detrimental effects of shear stress on cell viability.[164]

5.2. Unwanted Strand Fusion. Strand fusion refers to material spreading during the cross-linking or solidification phase after fabrication, resulting in the combination of adjacent strands and pore obstruction. Throughout the (bio)printing process, the newly deposited strands are not yet in their final state and require a cross-linking or cooling phase. During this intermediate phase, the material's rheological properties are critical. Specifically, the material viscosity dictates material spreading and the capacity to support the scaffold geometry while (bio)printing.[162] Further, material viscosities can be sorted into three categories: <300, ≤100 000, and >100 000 cP.[162] Of these categories, materials in the <300 cP range cannot properly retain their shape after fabrication.[162]

Additionally, the degree of cross-linking after the cross-linking process is vitally important to the strand's stability. In suboptimal cross-linking, the print material is more fluid and subsequently more apt to spread.[162,163] Naturally, undesirable print material viscosity or cross-linking degree leaves strands susceptible to spreading, leading to strand fusion (see Figure 9D).

The evaluation of strand fusion is in the form of postprint imaging coupled with image analysis.[102,162,163] While current strand fusion detection is done after the conclusion of a print, this allows strand fusion to compound throughout the print, resulting in an unusable print. As a result, in-process sensing of strand fusion would be a valuable development allowing for the detection, prevention, or even the remediation of this defect.

Through the works of Habib et al., the connection between a print material's rheology and its predisposition toward strand fusion was made by examining fusion between parallel strands at set spacings.[162,163] By looking into several hydrogel compositions, quantifying the material spread (diffusion rate) and printability, the works show that compositions with high viscosities at low shear stress had lower diffusion rates and

https://doi.org/10.1021/acsbiomaterials.1c00598
ACS Biomater. Sci. Eng. XXXX, XXX, XXX−XXX

higher printability values.[162,163] Similarly, Ribeiro et al. fabricated snaking architectures with set interstrand gaps and observed the severity of fusions between adjacent strands.[102] In the method presented by Ribeiro et al., the minimal interstrand gap resulting in similar strand and turnaround section widths was the critical distance below which there is significant strand and pore fusion.[102] An alternative method is to observe the average strand width to nozzle size ratio, otherwise known as the "spreading ratio".[167] Notably, these methods do not take a strand's as-deposited state into account, making them insensitive to whether spreading results from improper process parameters, material viscosity, or a combination of the two.

5.3. Strand Collapse. During the (bio)printing of porous geometries, pores are created as intentional void spaces within a layer and open spaces between the layers. The later vertical void spaces between layers require material to be placed across gaps in the previous layer. While (bio)printing over this overhang, it is possible for strands to maintain their shape, deflect, or breakdown entirely. This deflection or breakdown phenomenon is referred to as strand collapse and is dependent upon the print material's properties and the gap distance.[162,163] In hydrogel-based (bio)printing, the material's gelation is predominantly responsible for the ability to print over gaps.[162,163] When the extrusion exhibits a droplet-like flow, it signifies that under-gelation is occurring, and the material is in a more fluid state than in ideal gelation, leading to more severe strand collapse (see Figure 9C).[162,163] Comparatively, proper gelation can span reasonable gap sizes with minimal collapse (see Figure 9C).[162,163]

The determination of the occurrence and severity of strand collapse is mostly with postprint imaging.[162,163] Collapse severity can be quantified using equation 1, where the collapse factor (C_f) is the percent difference in the deflected area (A_a^c) versus the theoretical area under the strand (A_t).[162] Naturally, the higher the collapse factor, the more significant the difference between the actual and theoretical vertical pore area, signifying a higher degree of collapse severity. Additionally, strand collapse can be quantified by the angle of the strand's deflection at the suspended strand's edge.[102]

$$C_f = \frac{(A_t^c - A_a^c)}{A_t^c} \times 100\% \quad (1)$$

To mitigate the risk of strand collapse, it is necessary to not print over large gaps. However, gap distances large enough to facilitate strand collapse differ depending on the print material.[102,162,163] Therefore, it is necessary to experimentally determine the maximum gap a material can span with little to no deflection. To this end, a platform with specially distanced pillars is used, simulating several print scenarios.[102,162,163] Habib et al.'s works show that the chosen pillar distances are 1, 2, 3, 4, 5, and 6 mm, while Ribeiro et al. used distances of 1, 2, 4, 8, and 16 mm.[102,162,163] The material's critical gap distance can be determined through this method or with the collapse factor or deflection angle.[14,102,162,163] This critical gap distance can be defined as the largest distance that a strand can be printed over without significant deflection. The critical gap distance can then be used to design prints with gaps smaller than or equivalent to the critical gap distance and largely mitigate the risk of strand collapse.

5.4. Variability in Pore Geometry. During the (bio)printing process, small defects or the material's properties may cause nonuniformities or otherwise poor printability. (Bio)printing with a material and process parameter combination that displays large variability in strand diameter leads to the formation of nonuniform strands. As a result, nonuniform strands demonstrate edges that meander significantly, leading to a longer strand length than the theoretical length from the print design.[161] Further, nonuniform strands can alter the print's pore geometry from its theoretical shape (see Figure 9B).[161] Additionally, if the print material is in a more fluid state, it may be more predisposed to cohesion to previous layers, resulting in a change in pore geometry (see Figure 9B and D).[115,163] In multilayered constructs, meandering strands or material spread can lead to pore size reduction or even obstruction.

The detection of pore geometry and printability issues occurs through postlayer or postprint imaging, followed by image analysis for quantification of these defects.[115,161,163,168] However, because detection is currently only in postprocessing, there is no feedback during the process. As a result, the current means of prevention centers around optimizing process parameters and material properties to maximize print accuracy.

Pore quality quantification from postprint imaging is done through two main methods. First, intentional pore geometries can be quantified compared to their ideal geometry with equation 3 for circularity or equation 4 for square geometries.[14,115,161,163] These equations yield a value of 1 for near-perfect circles and squares, respectively. Second, overall print accuracy can be assessed using equation 5, relating the actual area taken up by the deposited strands to the theoretical design area.[168]

$$U = \frac{\text{length of printed strand}}{\text{length of the theoretical straight strand}} \quad (2)$$

$$\text{circularity} = \frac{4\pi \times \text{enclosed area}}{\text{enclosed perimeter}^2} \quad (3)$$

$$\text{square printability} = \frac{\text{enclosed perimeter}^2}{16 \times \text{enclosed area}} \quad (4)$$

$$\text{print accuracy} = \left[1 - \frac{|\text{printed area} - \text{theoretical area}|}{\text{theoretical area}}\right] \times 100\% \quad (5)$$

Process optimization is currently used to reduce these defects. In this approach, several variables, such as material composition, cross-linking condition, filament to filament distance, etc., can be varied to find a combination that yields the best quality.[115,161,163,168] For the analysis of strand uniformity and pore geometry, a perpendicularly opposed square grid design was used.[115,161] From a single layer of the print, strand uniformity can be determined by measuring the side lengths of a strand and using equation 2, with nonideal strands returning values in excess of $U = 1$.[161] In this way, strand uniformity can indicate that the pore quality of subsequent layers may be less than desirable, should the current meandering strands persist throughout the print.

After two perpendicularly placed layers, the grid of square pores is formed. Assessment is then conducted using equation 3 for circularity (yielding $\pi/4$ for a perfect square) or equation 4 (yielding 1 for a perfect square).[115,161,163] In either case, values that significantly differ from those targets indicate suboptimal printability, such as the circular or jagged geometries shown in Figure 9B.[115,161,163] Upon the completion

https://doi.org/10.1021/acsbiomaterials.1c00598
ACS Biomater. Sci. Eng. XXXX, XXX, XXX−XXX

of a print, the print accuracy may be determined through equation 5 to compare the printed area with the designed area.[168] Naturally, print accuracy has a maximum of 100%, and lower accuracies indicate suboptimal material or process parameters.

6. EFFECTS OF FLAWS ON MECHANICAL PROPERTIES OF PRINTED CONSTRUCTS

Naturally occurring tissues of the human body are primarily composite materials, possessing varying load-bearing capabilities. As a result, (bio)printed scaffolds must play a crucial role in providing suitable stiffness and mechanical signals to the cells to regulate their growing environment. The in vivo function of tissue-engineered scaffolds can be tailored by controlling properties, such as Young's modulus, toughness, and strength.[136]

The mechanical properties of implanted scaffolds are expected to closely match the mechanical properties of the surrounding tissues to achieve optimal clinical outcomes. For instance, bone scaffolds with weaker mechanical properties (<2−12 MPa compressive strength)[169] than the surrounding tissues can undergo premature mechanical failure.[170,171] In contrast, scaffolds stronger than the surrounding tissue shield the tissues from external loads, thus promoting tissue resorption.[170,171]

Similarly, if stiffer scaffolds than native tissue are used to treat soft tissue injuries (example native tissue stiffnesses; brain ∼100 Pa, liver ∼400 Pa, muscle ∼10 kPa),[172] severe fibrosis and a lack of tissue integration can occur. Thus, an ongoing goal of tissue engineering is to fabricate spatially controlled, heterogeneous patterns of pores throughout engineered scaffolds to mimic differences in mechanical requirements throughout the tissue.

The blending of several hydrogels has been increasingly used to develop (bio)inks, the biological and mechanical properties of which can be custom-tailored according to different requirements.[84,86] Naturally, reducing the concentration of a constituent, such as alginate from alginate/GelMA, will reduce the mechanical strength of the printed structure.[84,86] In the case of using a single hydrogel, the concentration of the hydrogel can directly be altered to achieve suitable mechanical properties. For instance, Rhee et al. observed that by increasing the concentration of the collagen hydrogel from to 20 mg/mL, the equilibrium modulus was increased to 30 kPa.[143] For reference, the actual human meniscus is around 75−125 kPa.[173]

However, while increasing hydrogel concentration can positively impact the mechanical strength, the change can negatively impact cell survivability and hydrogel printability. In the work of Bertassoni et al., a connection between elastic modulus and printability was proposed; below 1 kPa gels were unprintable; between 1.2 and 2.6 kPa was variable printability; above 2.6 kPa gels printed reproducibly. Bertassoni et al. also investigated the maximum load required for the piston to debond the hydrogel from the glass capillary and initiate dispensing. Generally, with a higher concentration of gels, the debonding required high loads.

In another study, Gerdes et al. investigated the occurrence of defects in a PCL/HAp matrix.[72] Several compositions of PCL/HAp were tested (70/30, 80/20, and 90/10 by PCL to HAp weight ratio). Further, a 60/40 composition was proved unviable because of its high viscosity, preventing extrusion even under the machine's highest temperature and pressure settings.[72] An in situ imaging system was utilized to assess the printability and geometric quality of the 3D printed scaffolds. Outside of printing, mechanical testing was conducted to determine material rheology and compressive moduli under different print parameters. Results from the mechanical testing showed trends of increasing viscosity with higher concentrations of HAp (negatively affecting printability) and the formation of less resilient scaffolds.[72] In addition, the in situ layer images suggested that defects propagated from improper printing can significantly lower the mechanical properties of 3D printed scaffold structures.[72]

This research vector requires thorough understanding to further develop due to the intimate relationship between flaws and the decreased mechanical and biological performance of (bio)printed scaffolds.

7. CONCLUSIONS AND FUTURE DIRECTIONS FOR RESEARCH

Bio-AM has emerged as a promising tool in regenerative medicine to solve various unmet medical needs. EBB has been the most popular Bio-AM strategy and has been extensively studied and utilized by various research groups. It is now widely accepted that the chemical, physical, and biological properties of the used (bio)inks and the formed scaffolds affect the biological outcome. For example, the printing quality depends on the rheological properties of the (bio)inks and the involved cross-linking process. Despite significant progress in the study of Bio-AM-based scaffolds in regenerative medicine applications, their translation into clinical practice has been limited. One of the critical areas most overlooked in the research efforts is the reproducibility of Bio-AM processes. Reproducibility is essential for assessing the suitability and safety of the products by regulatory agencies, such as the US Food and Drug Administration (FDA). Therefore, it is expected that more attention will be devoted to understanding material and architectural flaws and their production during Bio-AM processes. In addition, the effect of these flaws on the biological processes is not well explored. Furthermore, it is expected for research efforts to clarify the acceptable levels of defects that minimize negative impacts on the biological outcome.

The limited literature on the quality assessment of Bio-AM products and processes has focused on geometric integrity and resolution. Further work is also required to quantify defects in material composition, cellular concentration, and functionalization. In-process monitoring is currently focused on geometric integrity, neglecting the urgent need for in situ cell viability assessment. Our study demonstrated that there is currently no means of modeling fundamental process phenomena, such as distortion, cross-linking, and the layer-wise deposition of materials. Research efforts in this area are expected to pave the way to form Bio-AM scaffolds by design to meet the application requirements.

The translation of (bio)printed scaffolds requires systems that their function is predictable. For example, the scaffolds should seamlessly fit the defect site. Small geometrical changes may make the surgical procedure very challenging. In addition, defects can change the mechanical properties of the scaffolds and in specific applications this can be detrimental for their use. In most tissue engineering efforts, there is little control over the system post implantation and thus any unwanted structural, compositional, or biological flaws can lead to postsurgical complications.

https://doi.org/10.1021/acsbiomaterials.1c00598
ACS Biomater. Sci. Eng. XXXX, XXX, XXX−XXX

Another critical need for successful translation of Bio-AM tools is the lack of in situ process correction. In addition, the nondestructive characterization of Bio-AM constructs beyond the use of reporter cells is an urgent and unaddressed need. One of the emerging areas of Bio-AM is in situ and in vivo printing of scaffolds.[174,175] Researchers have developed many portable and stationary printers to enable direct printing in patients' bodies.[12,176,177] Currently, there are no quality control tools for these strategies, and this area is expected to be the subject of several research projects.

AUTHOR INFORMATION

Corresponding Authors

Ali Tamayol − *Department of Mechanical and Materials Engineering, University of Nebraska-Lincoln, Lincoln, Nebraska 68588-0526, United States; Department of Biomedical Engineering, University of Connecticut Health Center, Farmington, Connecticut 06269, United States;* orcid.org/0000-0003-1801-2889; Email: atamayol@uchc.edu

Iris V. Rivero − *Department of Industrial and Systems Engineering, Rochester Institute of Technology, Rochester, New York 14623, United States; Department of Biomedical Engineering, Rochester Institute of Technology, Rochester, New York 14623, United States*; Email: rao@unl.edu

Prahalada Rao − *Department of Mechanical and Materials Engineering, University of Nebraska-Lincoln, Lincoln, Nebraska 68588-0526, United States*; Email: iris.rivero@rit.edu

Authors

Samuel Gerdes − *Department of Mechanical and Materials Engineering, University of Nebraska-Lincoln, Lincoln, Nebraska 68588-0526, United States*

Srikanthan Ramesh − *Department of Industrial and Systems Engineering, Rochester Institute of Technology, Rochester, New York 14623, United States*

Azadeh Mostafavi − *Department of Mechanical and Materials Engineering, University of Nebraska-Lincoln, Lincoln, Nebraska 68588-0526, United States*

Complete contact information is available at: https://pubs.acs.org/10.1021/acsbiomaterials.1c00598

Notes

The authors declare no competing financial interest.

ACKNOWLEDGMENTS

Financial support from the National Science Foundation (NSF CMMI-1719388, CMMI-1739696, and CMMI-1752069), the National Institutes of Health (AR073822), the University of Nebraska-Lincoln, and Nebraska Tobacco Settlement Biomedical Research Enhancement Funds are gratefully acknowledged. Specifically, the concept of in situ imaging for process monitoring and assessing the effect of process conditions on quality of deposits in 3D (bio)printing of biomaterials was funded through CMMI-1739696 (Program Officer: Dr. Bruce Kramer).

REFERENCES

(1) Zhang, B.; Luo, Y.; Ma, L.; Gao, L.; Li, Y.; Xue, Q.; Yang, H.; Cui, Z. 3D Bioprinting: An Emerging Technology Full of Opportunities and Challenges. *Bio-Design Manuf.* **2018**, *1* (1), 2−13.

(2) Farzin, A.; Miri, A. K.; Sharifi, F.; Faramarzi, N.; Jaberi, A.; Mostafavi, A.; Solorzano, R.; Zhang, Y. S.; Annabi, N.; Khademhosseini, A.; Tamayol, A. 3D-Printed Sugar-Based Stents Facilitating Vascular Anastomosis. *Adv. Healthcare Mater.* **2018**, *7* (24), 1800702.

(3) Mandrycky, C.; Wang, Z.; Kim, K.; Kim, D.-H. 3D Bioprinting for Engineering Complex Tissues. *Biotechnol. Adv.* **2016**, *34* (4), 422−434.

(4) Faramarzi, N.; Yazdi, I. K.; Nabavinia, M.; Gemma, A.; Fanelli, A.; Caizzone, A.; Ptaszek, L. M.; Sinha, I.; Khademhosseini, A.; Ruskin, J. N.; Tamayol, A. Patient-Specific Bioinks for 3D Bioprinting of Tissue Engineering Scaffolds. *Adv. Healthcare Mater.* **2018**, *7* (11), 1701347.

(5) Zhu, K.; Shin, S. R.; van Kempen, T.; Li, Y.-C.; Ponraj, V.; Nasajpour, A.; Mandla, S.; Hu, N.; Liu, X.; Leijten, J.; Lin, Y.-D.; Hussain, M. A.; Zhang, Y. S.; Tamayol, A.; Khademhosseini, A. Gold Nanocomposite Bioink for Printing 3D Cardiac Constructs. *Adv. Funct. Mater.* **2017**, *27* (12), 1605352.

(6) Ostrovidov, S.; Salehi, S.; Costantini, M.; Suthiwanich, K.; Ebrahimi, M.; Sadeghian, R. B.; Fujie, T.; Shi, X.; Cannata, S.; Gargioli, C.; Tamayol, A.; Dokmeci, M. R.; Orive, G.; Swieszkowski, W.; Khademhosseini, A. 3D Bioprinting in Skeletal Muscle Tissue Engineering. *Small* **2019**, *15* (24), 1805530.

(7) Byambaa, B.; Annabi, N.; Yue, K.; Trujillo-de Santiago, G.; Alvarez, M. M.; Jia, W.; Kazemzadeh-Narbat, M.; Shin, S. R.; Tamayol, A.; Khademhosseini, A. Bioprinted Osteogenic and Vasculogenic Patterns for Engineering 3D Bone Tissue. *Adv. Healthcare Mater.* **2017**, *6* (16), 1700015.

(8) Gillispie, G.; Prim, P.; Copus, J.; Fisher, J.; Mikos, A. G.; Yoo, J. J.; Atala, A.; Lee, S. J. Assessment Methodologies for Extrusion-Based Bioink Printability. *Biofabrication* **2020**, *12* (2), 022003.

(9) Zhang, S.; Greenfield, M. A.; Mata, A.; Palmer, L. C.; Bitton, R.; Mantei, J. R.; Aparicio, C.; de la Cruz, M. O.; Stupp, S. I. A Self-Assembly Pathway to Aligned Monodomain Gels. *Nat. Mater.* **2010**, *9* (7), 594−601.

(10) Prince, E.; Kumacheva, E. Design and Applications of Man-Made Biomimetic Fibrillar Hydrogels. *Nat. Rev. Mater.* **2019**, *4* (2), 99−115.

(11) Samandari, M.; Alipanah, F.; Majidzadeh-A, K.; Alvarez, M. M.; Trujillo-de Santiago, G.; Tamayol, A. Controlling Cellular Organization in Bioprinting through Designed 3D Microcompartmentalization. *Appl. Phys. Rev.* **2021**, *8* (2), 021404.

(12) Russell, C. S.; Mostafavi, A.; Quint, J. P.; Panayi, A. C.; Baldino, K.; Williams, T. J.; Daubendiek, J. G.; Hugo Sánchez, V.; Bonick, Z.; Trujillo-Miranda, M.; Shin, S. R.; Pourquie, O.; Salehi, S.; Sinha, I.; Tamayol, A. In Situ Printing of Adhesive Hydrogel Scaffolds for the Treatment of Skeletal Muscle Injuries. *ACS Appl. Bio Mater.* **2020**, *3* (3), 1568−1579.

(13) Ramesh, S.; Harrysson, O. L. A.; Rao, P. K.; Tamayol, A.; Cormier, D. R.; Zhang, Y.; Rivero, I. V. Extrusion Bioprinting: Recent Progress, Challenges, and Future Opportunities. *Bioprinting* **2021**, *21*, No. e00116.

(14) Schwab, A.; Levato, R.; D'Este, M.; Piluso, S.; Eglin, D.; Malda, J. Printability and Shape Fidelity of Bioinks in 3D Bioprinting. *Chem. Rev.* **2020**, *120* (19), 11028−11055.

(15) Alves, N. M.; Pashkuleva, I.; Reis, R. L.; Mano, J. F. Controlling Cell Behavior Through the Design of Polymer Surfaces. *Small* **2010**, *6* (20), 2208−2220.

(16) Wolf, K.; Müller, R.; Borgmann, S.; Bröcker, E.-B.; Friedl, P. Amoeboid Shape Change and Contact Guidance: T-Lymphocyte Crawling through Fibrillar Collagen Is Independent of Matrix Remodeling by MMPs and Other Proteases. *Blood* **2003**, *102* (9), 3262−3269.

(17) Weiss, P. Experiments on Cell and Axon Orientation in Vitro: The Role of Colloidal Exudates in Tissue Organization. *J. Exp. Zool.* **1945**, *100* (3), 353−386.

(18) Elkhoury, K.; Russell, C. S.; Sanchez-Gonzalez, L.; Mostafavi, A.; Williams, T. J.; Kahn, C.; Peppas, N. A.; Arab-Tehrany, E.; Tamayol, A. Soft-Nanoparticle Functionalization of Natural Hydro-

gels for Tissue Engineering Applications. *Adv. Healthcare Mater.* **2019**, *8* (18), 1900506.
(19) Annabi, N.; Tamayol, A.; Uquillas, J. A.; Akbari, M.; Bertassoni, L. E.; Cha, C.; Camci-Unal, G.; Dokmeci, M. R.; Peppas, N. A.; Khademhosseini, A. 25th Anniversary Article: Rational Design and Applications of Hydrogels in Regenerative Medicine. *Adv. Mater.* **2014**, *26* (1), 85−124.
(20) Mohamed, M. A.; Fallahi, A.; El-Sokkary, A. M. A.; Salehi, S.; Akl, M. A.; Jafari, A.; Tamayol, A.; Fenniri, H.; Khademhosseini, A.; Andreadis, S. T.; Cheng, C. Stimuli-Responsive Hydrogels for Manipulation of Cell Microenvironment: From Chemistry to Biofabrication Technology. *Prog. Polym. Sci.* **2019**, *98*, 101147.
(21) Fallahi, A.; Yazdi, I. K.; Serex, L.; Lesha, E.; Faramarzi, N.; Tarlan, F.; Avci, H.; Costa-Almeida, R.; Sharifi, F.; Rinoldi, C.; Gomes, M. E.; Shin, S. R.; Khademhosseini, A.; Akbari, M.; Tamayol, A. Customizable Composite Fibers for Engineering Skeletal Muscle Models. *ACS Biomater. Sci. Eng.* **2020**, *6* (2), 1112−1123.
(22) Bettinger, C. J.; Langer, R.; Borenstein, J. T. Engineering Substrate Topography at the Micro- and Nanoscale to Control Cell Function. *Angew. Chem., Int. Ed.* **2009**, *48* (30), 5406−5415.
(23) Gui, N.; Xu, W.; Myers, D. E.; Shukla, R.; Tang, H. P.; Qian, M. The Effect of Ordered and Partially Ordered Surface Topography on Bone Cell Responses: A Review. *Biomater. Sci.* **2018**, *6* (2), 250−264.
(24) Kanchanawong, P.; Shtengel, G.; Pasapera, A. M.; Ramko, E. B.; Davidson, M. W.; Hess, H. F.; Waterman, C. M. Nanoscale Architecture of Integrin-Based Cell Adhesions. *Nature* **2010**, *468* (7323), 580−584.
(25) Que, L.; Topoleski, L. D. T. Surface Roughness Quantification of CoCrMo Implant Alloys. *J. Biomed. Mater. Res.* **1999**, *48* (5), 705−711.
(26) Khan, S. P.; Auner, G. G.; Newaz, G. M. Influence of Nanoscale Surface Roughness on Neural Cell Attachment on Silicon. *Nanomedicine* **2005**, *1* (2), 125−129.
(27) Pelipenko, J.; Kocbek, P.; Govedarica, B.; Rošic, R.; Baumgartner, S.; Kristl, J. The Topography of Electrospun Nanofibers and Its Impact on the Growth and Mobility of Keratinocytes. *Eur. J. Pharm. Biopharm.* **2013**, *84* (2), 401−411.
(28) Pelipenko, J.; Kocbek, P.; Kristl, J. Critical Attributes of Nanofibers: Preparation, Drug Loading, and Tissue Regeneration. *Int. J. Pharm.* **2015**, *484* (1), 57−74.
(29) Karuri, N. W.; Liliensiek, S.; Teixeira, A. I.; Abrams, G.; Campbell, S.; Nealey, P. F.; Murphy, C. J. Biological Length Scale Topography Enhances Cell-Substratum Adhesion of Human Corneal Epithelial Cells. *J. Cell Sci.* **2004**, *117* (15), 3153−3164.
(30) Goreham, R. V.; Mierczynska, A.; Smith, L. E.; Sedev, R.; Vasilev, K. Small Surface Nanotopography Encourages Fibroblast and Osteoblast Cell Adhesion. *RSC Adv.* **2013**, *3* (26), 10309−10317.
(31) Arnold, M.; Cavalcanti-Adam, E. A.; Glass, R.; Blümmel, J.; Eck, W.; Kantlehner, M.; Kessler, H.; Spatz, J. P. Activation of Integrin Function by Nanopatterned Adhesive Interfaces. *ChemPhysChem* **2004**, *5* (3), 383−388.
(32) Gulati, K.; Prideaux, M.; Kogawa, M.; Lima-Marques, L.; Atkins, G. J.; Findlay, D. M.; Losic, D. Anodized 3D−Printed Titanium Implants with Dual Micro- and Nano-Scale Topography Promote Interaction with Human Osteoblasts and Osteocyte-like Cells. *J. Tissue Eng. Regener. Med.* **2017**, *11* (12), 3313−3325.
(33) Dalby, M. J.; Riehle, M. O.; Johnstone, H. J. H.; Affrossman, S.; Curtis, A. S. G. Polymer-Demixed Nanotopography: Control of Fibroblast Spreading and Proliferation. *Tissue Eng.* **2002**, *8* (6), 1099−1108.
(34) Kim, D.-H.; Lipke, E. A.; Kim, P.; Cheong, R.; Thompson, S.; Delannoy, M.; Suh, K.-Y.; Tung, L.; Levchenko, A. Nanoscale Cues Regulate the Structure and Function of Macroscopic Cardiac Tissue Constructs. *Proc. Natl. Acad. Sci. U. S. A.* **2010**, *107* (2), 565−570.
(35) Lim, J. Y.; Dreiss, A. D.; Zhou, Z.; Hansen, J. C.; Siedlecki, C. A.; Hengstebeck, R. W.; Cheng, J.; Winograd, N.; Donahue, H. J. The Regulation of Integrin-Mediated Osteoblast Focal Adhesion and Focal Adhesion Kinase Expression by Nanoscale Topography. *Biomaterials* **2007**, *28* (10), 1787−1797.
(36) Oh, S.; Brammer, K. S.; Li, Y. S. J.; Teng, D.; Engler, A. J.; Chien, S.; Jin, S. Stem Cell Fate Dictated Solely by Altered Nanotube Dimension. *Proc. Natl. Acad. Sci. U. S. A.* **2009**, *106* (7), 2130−2135.
(37) Teo, B. K. K.; Wong, S. T.; Lim, C. K.; Kung, T. Y. S.; Yap, C. H.; Ramagopal, Y.; Romer, L. H.; Yim, E. K. F. Nanotopography Modulates Mechanotransduction of Stem Cells and Induces Differentiation through Focal Adhesion Kinase. *ACS Nano* **2013**, *7* (6), 4785−4798.
(38) Chaurey, V.; Block, F.; Su, Y.-H.; Chiang, P.-C.; Botchwey, E.; Chou, C.-F.; Swami, N. S. Nanofiber Size-Dependent Sensitivity of Fibroblast Directionality to the Methodology for Scaffold Alignment. *Acta Biomater.* **2012**, *8* (11), 3982−3990.
(39) Teixeira, A. I.; McKie, G. A.; Foley, J. D.; Bertics, P. J.; Nealey, P. F.; Murphy, C. J. The Effect of Environmental Factors on the Response of Human Corneal Epithelial Cells to Nanoscale Substrate Topography. *Biomaterials* **2006**, *27* (21), 3945−3954.
(40) Bhuthalingam, R.; Lim, P. Q.; Irvine, S. A.; Agrawal, A.; Mhaisalkar, P. S.; An, J.; Chua, C. K.; Venkatraman, S. A Novel 3D Printing Method for Cell Alignment and Differentiation. *Int. J. Bioprinting*; Vol *1*, 1 (2015)DO - 5765 **2015**.
(41) Liu, T.; Huang, R.; Zhong, J.; Yang, Y.; Tan, Z.; Tan, W. Control of Cell Proliferation in E-Jet 3D-Printed Scaffolds for Tissue Engineering Applications: The Influence of the Cell Alignment Angle. *J. Mater. Chem. B* **2017**, *5* (20), 3728−3738.
(42) Li, Y.; Xiao, Y.; Liu, C. The Horizon of Materiobiology: A Perspective on Material-Guided Cell Behaviors and Tissue Engineering. *Chem. Rev.* **2017**, *117* (5), 4376−4421.
(43) Kim, H. N.; Hong, Y.; Kim, M. S.; Kim, S. M.; Suh, K.-Y. Effect of Orientation and Density of Nanotopography in Dermal Wound Healing. *Biomaterials* **2012**, *33* (34), 8782−8792.
(44) Kim, D.-H.; Seo, C.-H.; Han, K.; Kwon, K. W.; Levchenko, A.; Suh, K.-Y. Guided Cell Migration on Microtextured Substrates with Variable Local Density and Anisotropy. *Adv. Funct. Mater.* **2009**, *19* (10), 1579−1586.
(45) Mahmud, G.; Campbell, C. J.; Bishop, K. J. M.; Komarova, Y. A.; Chaga, O.; Soh, S.; Huda, S.; Kandere-Grzybowska, K.; Grzybowski, B. A. Directing Cell Motions on Micropatterned Ratchets. *Nat. Phys.* **2009**, *5* (8), 606−612.
(46) Prasopthum, A.; Shakesheff, K. M.; Yang, J. Direct Three-Dimensional Printing of Polymeric Scaffolds with Nanofibrous Topography. *Biofabrication* **2018**, *10* (2), 025002.
(47) Smith, A. M.; Paxton, J. Z.; Hung, Y.-P.; Hadley, M. J.; Bowen, J.; Williams, R. L.; Grover, L. M. Nanoscale Crystallinity Modulates Cell Proliferation on Plasma Sprayed Surfaces. *Mater. Sci. Eng., C* **2015**, *48*, 5−10.
(48) Gentile, F.; Medda, R.; Cheng, L.; Battista, E.; Scopelliti, P. E.; Milani, P.; Cavalcanti-Adam, E. A.; Decuzzi, P. Selective Modulation of Cell Response on Engineered Fractal Silicon Substrates. *Sci. Rep.* **2013**, *3* (1), 1461.
(49) Hoveizi, E.; Ebrahimi-Barough, S.; Tavakol, S.; Nabiuni, M. Vitro Comparative Survey of Cell Adhesion and Proliferation of Human Induced Pluripotent Stem Cells on Surfaces of Polymeric Electrospun Nanofibrous and Solution-Cast Film Scaffolds. *J. Biomed. Mater. Res., Part A* **2015**, *103* (9), 2952−2958.
(50) Park, J.; Bauer, S.; von der Mark, K.; Schmuki, P. Nanosize and Vitality: TiO_2 Nanotube Diameter Directs Cell Fate. *Nano Lett.* **2007**, *7* (6), 1686−1691.
(51) Janson, I. A.; Kong, Y. P.; Putnam, A. J. Nanotopographic Substrates of Poly (Methyl Methacrylate) Do Not Strongly Influence the Osteogenic Phenotype of Mesenchymal Stem Cells in Vitro. *PLoS One* **2014**, *9* (3), e90719.
(52) Rebollar, E.; Frischauf, I.; Olbrich, M.; Peterbauer, T.; Hering, S.; Preiner, J.; Hinterdorfer, P.; Romanin, C.; Heitz, J. Proliferation of Aligned Mammalian Cells on Laser-Nanostructured Polystyrene. *Biomaterials* **2008**, *29* (12), 1796−1806.
(53) Han, G.; Müller, W. E. G.; Wang, X.; Lilja, L.; Shen, Z. Porous Titania Surfaces on Titanium with Hierarchical Macro- and Mesoporosities for Enhancing Cell Adhesion, Proliferation and Mineralization. *Mater. Sci. Eng., C* **2015**, *47*, 376−383.

https://doi.org/10.1021/acsbiomaterials.1c00598
ACS Biomater. Sci. Eng. XXXX, XXX, XXX−XXX

(54) Tanaka, T.; Suzuki, Y. Spatial Control of Cell Attachment, Proliferation, and Differentiation Using Ion-Beam Induced Thin Films. *Appl. Surf. Sci.* **2014**, *310*, 31−35.
(55) Lim, S. H.; Liu, X. Y.; Song, H.; Yarema, K. J.; Mao, H.-Q. The Effect of Nanofiber-Guided Cell Alignment on the Preferential Differentiation of Neural Stem Cells. *Biomaterials* **2010**, *31* (34), 9031−9039.
(56) Yim, E. K. F.; Pang, S. W.; Leong, K. W. Synthetic Nanostructures Inducing Differentiation of Human Mesenchymal Stem Cells into Neuronal Lineage. *Exp. Cell Res.* **2007**, *313* (9), 1820−1829.
(57) Dang, J. M.; Leong, K. W. Myogenic Induction of Aligned Mesenchymal Stem Cell Sheets by Culture on Thermally Responsive Electrospun Nanofibers. *Adv. Mater.* **2007**, *19* (19), 2775−2779.
(58) Dalby, M. J.; Gadegaard, N.; Tare, R.; Andar, A.; Riehle, M. O.; Herzyk, P.; Wilkinson, C. D. W.; Oreffo, R. O. C. The Control of Human Mesenchymal Cell Differentiation Using Nanoscale Symmetry and Disorder. *Nat. Mater.* **2007**, *6* (12), 997−1003.
(59) Abadi, P. P. S. S.; Garbern, J. C.; Behzadi, S.; Hill, M. J.; Tresback, J. S.; Heydari, T.; Ejtehadi, M. R.; Ahmed, N.; Copley, E.; Aghaverdi, H.; Lee, R. T.; Farokhzad, O. C.; Mahmoudi, M. Engineering of Mature Human Induced Pluripotent Stem Cell-Derived Cardiomyocytes Using Substrates with Multiscale Topography. *Adv. Funct. Mater.* **2018**, *28* (19), 1707378.
(60) Kilian, K. A.; Bugarija, B.; Lahn, B. T.; Mrksich, M. Geometric Cues for Directing the Differentiation of Mesenchymal Stem Cells. *Proc. Natl. Acad. Sci. U. S. A.* **2010**, *107* (11), 4872−4877.
(61) Discher, D. E.; Janmey, P.; Wang, Y. Tissue Cells Feel and Respond to the Stiffness of Their Substrate. *Science (Washington, DC, U. S.)* **2005**, *310* (5751), 1139−1143.
(62) Petrie, R. J.; Yamada, K. M. At the Leading Edge of Three-Dimensional Cell Migration. *J. Cell Sci.* **2012**, *125* (24), 5917−5926.
(63) Koch, T. M.; Münster, S.; Bonakdar, N.; Butler, J. P.; Fabry, B. 3D Traction Forces in Cancer Cell Invasion. *PLoS One* **2012**, *7* (3), e33476.
(64) Liu, W.; Lipner, J.; Xie, J.; Manning, C. N.; Thomopoulos, S.; Xia, Y. Nanofiber Scaffolds with Gradients in Mineral Content for Spatial Control of Osteogenesis. *ACS Appl. Mater. Interfaces* **2014**, *6* (4), 2842−2849.
(65) Engler, A. J.; Sen, S.; Sweeney, H. L.; Discher, D. E. Matrix Elasticity Directs Stem Cell Lineage Specification. *Cell* **2006**, *126* (4), 677−689.
(66) Pan, T.; Song, W.; Cao, X.; Wang, Y. 3D Bioplotting of Gelatin/Alginate Scaffolds for Tissue Engineering: Influence of Crosslinking Degree and Pore Architecture on Physicochemical Properties. *J. Mater. Sci. Technol.* **2016**, *32* (9), 889−900.
(67) Zhang, J.; Ma, X.; Lin, D.; Shi, H.; Yuan, Y.; Tang, W.; Zhou, H.; Guo, H.; Qian, J.; Liu, C. Magnesium Modification of a Calcium Phosphate Cement Alters Bone Marrow Stromal Cell Behavior via an Integrin-Mediated Mechanism. *Biomaterials* **2015**, *53*, 251−264.
(68) Dubin-Thaler, B. J.; Giannone, G.; Döbereiner, H.-G.; Sheetz, M. P. Nanometer Analysis of Cell Spreading on Matrix-Coated Surfaces Reveals Two Distinct Cell States and STEPs. *Biophys. J.* **2004**, *86* (3), 1794−1806.
(69) Arima, Y.; Iwata, H. Effect of Wettability and Surface Functional Groups on Protein Adsorption and Cell Adhesion Using Well-Defined Mixed Self-Assembled Monolayers. *Biomaterials* **2007**, *28* (20), 3074−3082.
(70) Lee, J. H.; Shin, Y. C.; Jin, O. S.; Kang, S. H.; Hwang, Y.-S.; Park, J.-C.; Hong, S. W.; Han, D.-W. Reduced Graphene Oxide-Coated Hydroxyapatite Composites Stimulate Spontaneous Osteogenic Differentiation of Human Mesenchymal Stem Cells. *Nanoscale* **2015**, *7* (27), 11642−11651.
(71) Li, H.; Xue, K.; Kong, N.; Liu, K.; Chang, J. Silicate Bioceramics Enhanced Vascularization and Osteogenesis through Stimulating Interactions between Endothelia Cells and Bone Marrow Stromal Cells. *Biomaterials* **2014**, *35* (12), 3803−3818.
(72) Gerdes, S.; Mostafavi, A.; Ramesh, S.; Memic, A.; Rivero, I. V.; Rao, P.; Tamayol, A. Process−Structure−Quality Relationships of Three-Dimensional Printed Poly(Caprolactone)-Hydroxyapatite Scaffolds. *Tissue Eng., Part A* **2020**, *26* (5−6), 279−291.
(73) DeForest, C. A.; Anseth, K. S. Advances in Bioactive Hydrogels to Probe and Direct Cell Fate. *Annu. Rev. Chem. Biomol. Eng.* **2012**, *3* (1), 421−444.
(74) Ulrich, T. A.; Jain, A.; Tanner, K.; MacKay, J. L.; Kumar, S. Probing Cellular Mechanobiology in Three-Dimensional Culture with Collagen−Agarose Matrices. *Biomaterials* **2010**, *31* (7), 1875−1884.
(75) Peyton, S. R.; Kalcioglu, Z. I.; Cohen, J. C.; Runkle, A. P.; Van Vliet, K. J.; Lauffenburger, D. A.; Griffith, L. G. Marrow-Derived Stem Cell Motility in 3D Synthetic Scaffold Is Governed by Geometry along with Adhesivity and Stiffness. *Biotechnol. Bioeng.* **2011**, *108* (5), 1181−1193.
(76) Ferlin, K. M.; Prendergast, M. E.; Miller, M. L.; Kaplan, D. S.; Fisher, J. P. Influence of 3D Printed Porous Architecture on Mesenchymal Stem Cell Enrichment and Differentiation. *Acta Biomater.* **2016**, *32*, 161−169.
(77) Baker, B. M.; Chen, C. S. Deconstructing the Third Dimension—How 3D Culture Microenvironments Alter Cellular Cues. *J. Cell Sci.* **2012**, *125* (13), 3015−3024.
(78) Müller, M.; Becher, J.; Schnabelrauch, M.; Zenobi-Wong, M. Nanostructured Pluronic Hydrogels as Bioinks for 3D Bioprinting. *Biofabrication* **2015**, *7* (3), 035006.
(79) Wu, D.; Yu, Y.; Tan, J.; Huang, L.; Luo, B.; Lu, L.; Zhou, C. 3D Bioprinting of Gellan Gum and Poly (Ethylene Glycol) Diacrylate Based Hydrogels to Produce Human-Scale Constructs with High-Fidelity. *Mater. Des.* **2018**, *160*, 486−495.
(80) Ghorbanian, S.; Qasaimeh, M. A.; Akbari, M.; Tamayol, A.; Juncker, D. Microfluidic Direct Writer with Integrated Declogging Mechanism for Fabricating Cell-Laden Hydrogel Constructs. *Biomed. Microdevices* **2014**, *16* (3), 387−395.
(81) Lee, W.; Debasitis, J. C.; Lee, V. K.; Lee, J.-H.; Fischer, K.; Edminster, K.; Park, J.-K.; Yoo, S.-S. Multi-Layered Culture of Human Skin Fibroblasts and Keratinocytes through Three-Dimensional Freeform Fabrication. *Biomaterials* **2009**, *30* (8), 1587−1595.
(82) Duarte Campos, D. F.; Blaeser, A.; Korsten, A.; Neuss, S.; Jäkel, J.; Vogt, M.; Fischer, H. The Stiffness and Structure of Three-Dimensional Printed Hydrogels Direct the Differentiation of Mesenchymal Stromal Cells Toward Adipogenic and Osteogenic Lineages. *Tissue Eng., Part A* **2015**, *21* (3−4), 740−756.
(83) Kolesky, D. B.; Homan, K. A.; Skylar-Scott, M. A.; Lewis, J. A. Three-Dimensional Bioprinting of Thick Vascularized Tissues. *Proc. Natl. Acad. Sci. U. S. A.* **2016**, *113* (12), 3179−3184.
(84) Tamayol, A.; Najafabadi, A. H.; Aliakbarian, B.; Arab-Tehrany, E.; Akbari, M.; Annabi, N.; Juncker, D.; Khademhosseini, A. Hydrogel Templates for Rapid Manufacturing of Bioactive Fibers and 3D Constructs. *Adv. Healthcare Mater.* **2015**, *4* (14), 2146−2153.
(85) Ma, X.; Yu, C.; Wang, P.; Xu, W.; Wan, X.; Lai, C. S. E.; Liu, J.; Koroleva-Maharajh, A.; Chen, S. Rapid 3D Bioprinting of Decellularized Extracellular Matrix with Regionally Varied Mechanical Properties and Biomimetic Microarchitecture. *Biomaterials* **2018**, *185*, 310−321.
(86) Jia, W.; Gungor-Ozkerim, P. S.; Zhang, Y. S.; Yue, K.; Zhu, K.; Liu, W.; Pi, Q.; Byambaa, B.; Dokmeci, M. R.; Shin, S. R.; Khademhosseini, A. Direct 3D Bioprinting of Perfusable Vascular Constructs Using a Blend Bioink. *Biomaterials* **2016**, *106*, 58−68.
(87) Shi, L.; Carstensen, H.; Hölzl, K.; Lunzer, M.; Li, H.; Hilborn, J.; Ovsianikov, A.; Ossipov, D. A. Dynamic Coordination Chemistry Enables Free Directional Printing of Biopolymer Hydrogel. *Chem. Mater.* **2017**, *29* (14), 5816−5823.
(88) Wüst, S.; Godla, M. E.; Müller, R.; Hofmann, S. Tunable Hydrogel Composite with Two-Step Processing in Combination with Innovative Hardware Upgrade for Cell-Based Three-Dimensional Bioprinting. *Acta Biomater.* **2014**, *10* (2), 630−640.
(89) Bertassoni, L. E.; Cecconi, M.; Manoharan, V.; Nikkhah, M.; Hjortnaes, J.; Cristino, A. L.; Barabaschi, G.; Demarchi, D.; Dokmeci, M. R.; Yang, Y.; Khademhosseini, A. Hydrogel Bioprinted Microchannel Networks for Vascularization of Tissue Engineering Constructs. *Lab Chip* **2014**, *14* (13), 2202−2211.

https://doi.org/10.1021/acsbiomaterials.1c00598
ACS Biomater. Sci. Eng. XXXX, XXX, XXX−XXX

(90) Malda, J.; Visser, J.; Melchels, F. P.; Jüngst, T.; Hennink, W. E.; Dhert, W. J. A.; Groll, J.; Hutmacher, D. W. 25th Anniversary Article: Engineering Hydrogels for Biofabrication. *Adv. Mater.* **2013**, *25* (36), 5011−5028.
(91) Gudapati, H.; Dey, M.; Ozbolat, I. A Comprehensive Review on Droplet-Based Bioprinting: Past, Present and Future. *Biomaterials* **2016**, *102*, 20−42.
(92) Chen, N.; Zhu, K.; Zhang, Y. S.; Yan, S.; Pan, T.; Abudupataer, M.; Yu, G.; Alam, M. F.; Wang, L.; Sun, X.; Yu, Y.; Wang, C.; Zhang, W. Hydrogel Bioink with Multilayered Interfaces Improves Dispersibility of Encapsulated Cells in Extrusion Bioprinting. *ACS Appl. Mater. Interfaces* **2019**, *11* (34), 30585−30595.
(93) Ashammakhi, N.; Ahadian, S.; Xu, C.; Montazerian, H.; Ko, H.; Nasiri, R.; Barros, N.; Khademhosseini, A. Bioinks and Bioprinting Technologies to Make Heterogeneous and Biomimetic Tissue Constructs. *Mater. Today Bio* **2019**, *1*, 100008.
(94) Zwanzig, R.; Harrison, A. K. Modifications of the Stokes−Einstein Formula. *J. Chem. Phys.* **1985**, *83* (11), 5861−5862.
(95) Saunders, R. E.; Gough, J. E.; Derby, B. Delivery of Human Fibroblast Cells by Piezoelectric Drop-on-Demand Inkjet Printing. *Biomaterials* **2008**, *29* (2), 193−203.
(96) Dababneh, A. B.; Ozbolat, I. T. Bioprinting Technology: A Current State-of-the-Art Review. *J. Manuf. Sci. Eng.* **2014**, DOI: 10.1115/1.4028512.
(97) He, Y.; Yang, F.; Zhao, H.; Gao, Q.; Xia, B.; Fu, J. Research on the Printability of Hydrogels in 3D Bioprinting. *Sci. Rep.* **2016**, *6* (1), 29977.
(98) Skardal, A. Perspective: "Universal" Bioink Technology for Advancing Extrusion Bioprinting-Based Biomanufacturing. *Bioprinting* **2018**, *10*, No. e00026.
(99) Jin, Y.; Chai, W.; Huang, Y. Printability Study of Hydrogel Solution Extrusion in Nanoclay Yield-Stress Bath during Printing-Then-Gelation Biofabrication. *Mater. Sci. Eng., C* **2017**, *80*, 313−325.
(100) Jia, J.; Richards, D. J.; Pollard, S.; Tan, Y.; Rodriguez, J.; Visconti, R. P.; Trusk, T. C.; Yost, M. J.; Yao, H.; Markwald, R. R.; Mei, Y. Engineering Alginate as Bioink for Bioprinting. *Acta Biomater.* **2014**, *10* (10), 4323−4331.
(101) Paxton, N.; Smolan, W.; Böck, T.; Melchels, F.; Groll, J.; Jungst, T. Proposal to Assess Printability of Bioinks for Extrusion-Based Bioprinting and Evaluation of Rheological Properties Governing Bioprintability. *Biofabrication* **2017**, *9* (4), 044107.
(102) Ribeiro, A.; Blokzijl, M. M.; Levato, R.; Visser, C. W.; Castilho, M.; Hennink, W. E.; Vermonden, T.; Malda, J. Assessing Bioink Shape Fidelity to Aid Material Development in 3D Bioprinting. *Biofabrication* **2018**, *10* (1), 014102.
(103) Hinton, T. J.; Jallerat, Q.; Palchesko, R. N.; Park, J. H.; Grodzicki, M. S.; Shue, H.-J.; Ramadan, M. H.; Hudson, A. R.; Feinberg, A. W. Three-Dimensional Printing of Complex Biological Structures by Freeform Reversible Embedding of Suspended Hydrogels. *Sci. Adv.* **2015**, *1* (9), No. e1500758.
(104) Lee, A.; Hudson, A. R.; Shiwarski, D. J.; Tashman, J. W.; Hinton, T. J.; Yerneni, S.; Bliley, J. M.; Campbell, P. G.; Feinberg, A. W. 3D Bioprinting of Collagen to Rebuild Components of the Human Heart. *Science (Washington, DC, U. S.)* **2019**, *365* (6452), 482−487.
(105) Mirdamadi, E.; Tashman, J. W.; Shiwarski, D. J.; Palchesko, R. N.; Feinberg, A. W. FRESH 3D Bioprinting a Full-Size Model of the Human Heart. *ACS Biomater. Sci. Eng.* **2020**, *6* (11), 6453−6459.
(106) Ning, L.; Gil, C. J.; Hwang, B.; Theus, A. S.; Perez, L.; Tomov, M. L.; Bauser-Heaton, H.; Serpooshan, V. Biomechanical Factors in Three-Dimensional Tissue Bioprinting. *Appl. Phys. Rev.* **2020**, *7* (4), 041319.
(107) Gao, T.; Gillispie, G. J.; Copus, J. S.; PR, A. K.; Seol, Y.-J.; Atala, A.; Yoo, J. J.; Lee, S. J. Optimization of Gelatin−Alginate Composite Bioink Printability Using Rheological Parameters: A Systematic Approach. *Biofabrication* **2018**, *10* (3), 034106.
(108) Wu, Y.; Lin, Z. Y.; Wenger, A. C.; Tam, K. C.; Tang, X. 3D Bioprinting of Liver-Mimetic Construct with Alginate/Cellulose Nanocrystal Hybrid Bioink. *Bioprinting* **2018**, *9*, 1−6.
(109) Banerjee, A.; Arha, M.; Choudhary, S.; Ashton, R. S.; Bhatia, S. R.; Schaffer, D. V.; Kane, R. S. The Influence of Hydrogel Modulus on the Proliferation and Differentiation of Encapsulated Neural Stem Cells. *Biomaterials* **2009**, *30* (27), 4695−4699.
(110) Blaeser, A.; Duarte Campos, D. F.; Puster, U.; Richtering, W.; Stevens, M. M.; Fischer, H. Controlling Shear Stress in 3D Bioprinting Is a Key Factor to Balance Printing Resolution and Stem Cell Integrity. *Adv. Healthcare Mater.* **2016**, *5* (3), 326−333.
(111) Ning, L.; Betancourt, N.; Schreyer, D. J.; Chen, X. Characterization of Cell Damage and Proliferative Ability during and after Bioprinting. *ACS Biomater. Sci. Eng.* **2018**, *4* (11), 3906−3918.
(112) Hong, S.; Sycks, D.; Chan, H. F.; Lin, S.; Lopez, G. P.; Guilak, F.; Leong, K. W.; Zhao, X. 3D Printing of Highly Stretchable and Tough Hydrogels into Complex, Cellularized Structures. *Adv. Mater.* **2015**, *27* (27), 4035−4040.
(113) Nair, K.; Gandhi, M.; Khalil, S.; Yan, K. C.; Marcolongo, M.; Barbee, K.; Sun, W. Characterization of Cell Viability during Bioprinting Processes. *Biotechnol. J.* **2009**, *4* (8), 1168−1177.
(114) Billiet, T.; Gevaert, E.; De Schryver, T.; Cornelissen, M.; Dubruel, P. The 3D Printing of Gelatin Methacrylamide Cell-Laden Tissue-Engineered Constructs with High Cell Viability. *Biomaterials* **2014**, *35* (1), 49−62.
(115) Ouyang, L.; Yao, R.; Zhao, Y.; Sun, W. Effect of Bioink Properties on Printability and Cell Viability for 3D Bioplotting of Embryonic Stem Cells. *Biofabrication* **2016**, *8* (3), 035020.
(116) Müller, M.; Öztürk, E.; Arlov, Ø.; Gatenholm, P.; Zenobi-Wong, M. Alginate Sulfate−Nanocellulose Bioinks for Cartilage Bioprinting Applications. *Ann. Biomed. Eng.* **2017**, *45* (1), 210−223.
(117) Ho, L.; Hsu, S.-H. Cell Reprogramming by 3D Bioprinting of Human Fibroblasts in Polyurethane Hydrogel for Fabrication of Neural-like Constructs. *Acta Biomater.* **2018**, *70*, 57−70.
(118) Lee, S. C.; Gillispie, G.; Prim, P.; Lee, S. J. Physical and Chemical Factors Influencing the Printability of Hydrogel-Based Extrusion Bioinks. *Chem. Rev.* **2020**, *120* (19), 10834−10886.
(119) Bertassoni, L. E.; Cardoso, J. C.; Manoharan, V.; Cristino, A. L.; Bhise, N. S.; Araujo, W. A.; Zorlutuna, P.; Vrana, N. E.; Ghaemmaghami, A. M.; Dokmeci, M. R.; Khademhosseini, A. Direct-Write Bioprinting of Cell-Laden Methacrylated Gelatin Hydrogels. *Biofabrication* **2014**, *6* (2), 024105.
(120) Yin, J.; Yan, M.; Wang, Y.; Fu, J.; Suo, H. 3D Bioprinting of Low-Concentration Cell-Laden Gelatin Methacrylate (GelMA) Bioinks with a Two-Step Cross-Linking Strategy. *ACS Appl. Mater. Interfaces* **2018**, *10* (8), 6849−6857.
(121) You, F.; Eames, B. F.; Chen, X. Application of Extrusion-Based Hydrogel Bioprinting for Cartilage Tissue Engineering. *Int. J. Mol. Sci.* **2017**, *18*, 1597.
(122) Wilson, S. A.; Cross, L. M.; Peak, C. W.; Gaharwar, A. K. Shear-Thinning and Thermo-Reversible Nanoengineered Inks for 3D Bioprinting. *ACS Appl. Mater. Interfaces* **2017**, *9* (50), 43449−43458.
(123) Shin, S.; Park, S.; Park, M.; Jeong, E.; Na, K.; Youn, H. J.; Hyun, J. Cellulose Nanofibers for the Enhancement of Printability of Low Viscosity Gelatin Derivatives. *BioResources* **2017**, DOI: 10.15376/biores.12.2.2941-2954.
(124) AnilKumar, S.; Allen, S. C.; Tasnim, N.; Akter, T.; Park, S.; Kumar, A.; Chattopadhyay, M.; Ito, Y.; Suggs, L. J.; Joddar, B. The Applicability of Furfuryl-Gelatin as a Novel Bioink for Tissue Engineering Applications. *J. Biomed. Mater. Res., Part B* **2019**, *107* (2), 314−323.
(125) Kesti, M.; Müller, M.; Becher, J.; Schnabelrauch, M.; D'Este, M.; Eglin, D.; Zenobi-Wong, M. A Versatile Bioink for Three-Dimensional Printing of Cellular Scaffolds Based on Thermally and Photo-Triggered Tandem Gelation. *Acta Biomater.* **2015**, *11*, 162−172.
(126) Tan, E. Y. S.; Yeong, W. Y. Concentric Bioprinting of Alginate-Based Tubular Constructs Using Multi-Nozzle Extrusion-Based Technique. *Int. J. Bioprinting* **2015**, *1* (1), No. 01003.
(127) Markstedt, K.; Mantas, A.; Tournier, I.; Martínez Ávila, H.; Hägg, D.; Gatenholm, P. 3D Bioprinting Human Chondrocytes with

Nanocellulose−Alginate Bioink for Cartilage Tissue Engineering Applications. *Biomacromolecules* **2015**, *16* (5), 1489−1496.
(128) Nguyen, D.; Hägg, D. A.; Forsman, A.; Ekholm, J.; Nimkingratana, P.; Brantsing, C.; Kalogeropoulos, T.; Zaunz, S.; Concaro, S.; Brittberg, M.; Lindahl, A.; Gatenholm, P.; Enejder, A.; Simonsson, S. Cartilage Tissue Engineering by the 3D Bioprinting of IPS Cells in a Nanocellulose/Alginate Bioink. *Sci. Rep.* **2017**, *7* (1), 658.
(129) Martínez Ávila, H.; Schwarz, S.; Rotter, N.; Gatenholm, P. 3D Bioprinting of Human Chondrocyte-Laden Nanocellulose Hydrogels for Patient-Specific Auricular Cartilage Regeneration. *Bioprinting* **2016**, *1*−*2*, 22−35.
(130) Irvine, S. A.; Agrawal, A.; Lee, B. H.; Chua, H. Y.; Low, K. Y.; Lau, B. C.; Machluf, M.; Venkatraman, S. Printing Cell-Laden Gelatin Constructs by Free-Form Fabrication and Enzymatic Protein Crosslinking. *Biomed. Microdevices* **2015**, *17* (1), 16.
(131) Censi, R.; Schuurman, W.; Malda, J.; di Dato, G.; Burgisser, P. E.; Dhert, W. J. A.; van Nostrum, C. F.; di Martino, P.; Vermonden, T.; Hennink, W. E. A Printable Photopolymerizable Thermosensitive p(HPMAm-Lactate)-PEG Hydrogel for Tissue Engineering. *Adv. Funct. Mater.* **2011**, *21* (10), 1833−1842.
(132) Skardal, A.; Zhang, J.; McCoard, L.; Xu, X.; Oottamasathien, S.; Prestwich, G. D. Photocrosslinkable Hyaluronan-Gelatin Hydrogels for Two-Step Bioprinting. *Tissue Eng., Part A* **2010**, *16* (8), 2675−2685.
(133) Ouyang, L.; Highley, C. B.; Rodell, C. B.; Sun, W.; Burdick, J. A. 3D Printing of Shear-Thinning Hyaluronic Acid Hydrogels with Secondary Cross-Linking. *ACS Biomater. Sci. Eng.* **2016**, *2* (10), 1743−1751.
(134) Jia, X.; Kiick, K. L. Hybrid Multicomponent Hydrogels for Tissue Engineering. *Macromol. Biosci.* **2009**, *9* (2), 140−156.
(135) Park, J.; Lee, S. J.; Chung, S.; Lee, J. H.; Kim, W. D.; Lee, J. Y.; Park, S. A. Cell-Laden 3D Bioprinting Hydrogel Matrix Depending on Different Compositions for Soft Tissue Engineering: Characterization and Evaluation. *Mater. Sci. Eng., C* **2017**, *71*, 678−684.
(136) Schuurman, W.; Khristov, V.; Pot, M. W.; van Weeren, P. R.; Dhert, W. J. A.; Malda, J. Bioprinting of Hybrid Tissue Constructs with Tailorable Mechanical Properties. *Biofabrication* **2011**, *3* (2), 021001.
(137) Zhang, K.; Fu, Q.; Yoo, J.; Chen, X.; Chandra, P.; Mo, X.; Song, L.; Atala, A.; Zhao, W. 3D Bioprinting of Urethra with PCL/PLCL Blend and Dual Autologous Cells in Fibrin Hydrogel: An in Vitro Evaluation of Biomimetic Mechanical Property and Cell Growth Environment. *Acta Biomater.* **2017**, *50*, 154−164.
(138) Kundu, J.; Shim, J. H.; Jang, J.; Kim, S. W.; Cho, D. W. An Additive Manufacturing-Based PCL-Alginate-Chondrocyte Bioprinted Scaffold for Cartilage Tissue Engineering. *J. Tissue Eng. Regener. Med.* **2015**, *9*, 1286.
(139) Kolesky, D. B.; Homan, K. A.; Skylar-Scott, M. A.; Lewis, J. A. Three-Dimensional Bioprinting of Thick Vascularized Tissues. *Proc. Natl. Acad. Sci. U. S. A.* **2016**, *113*, 3179.
(140) Tan, E. Y. S.; Yeong, W. Y. Concentric Bioprinting of Alginate-Based Tubular Constructs Using Multi-Nozzle Extrusion-Based Technique. *Int. J. Bioprinting* **2015**, DOI: 10.18063/IJB.2015.01.003.
(141) Khalil, S.; Sun, W. Bioprinting Endothelial Cells With Alginate for 3D Tissue Constructs. *J. Biomech. Eng.* **2009**, DOI: 10.1115/1.3128729.
(142) Kang, H. W.; Lee, S. J.; Ko, I. K.; Kengla, C.; Yoo, J. J.; Atala, A. A 3D Bioprinting System to Produce Human-Scale Tissue Constructs with Structural Integrity. *Nat. Biotechnol.* **2016**, *34*, 312.
(143) Rhee, S.; Puetzer, J. L.; Mason, B. N.; Reinhart-King, C. A.; Bonassar, L. J. 3D Bioprinting of Spatially Heterogeneous Collagen Constructs for Cartilage Tissue Engineering. *ACS Biomater. Sci. Eng.* **2016**, *2* (10), 1800−1805.
(144) Lee, V.; Singh, G.; Trasatti, J. P.; Bjornsson, C.; Xu, X.; Tran, T. N.; Yoo, S.-S.; Dai, G.; Karande, P. Design and Fabrication of Human Skin by Three-Dimensional Bioprinting. *Tissue Eng., Part C* **2014**, *20* (6), 473−484.
(145) Hutmacher, D. W.; Schantz, T.; Zein, I.; Ng, K. W.; Teoh, S. H.; Tan, K. C. Mechanical Properties and Cell Cultural Response of Polycaprolactone Scaffolds Designed and Fabricated via Fused Deposition Modeling. *J. Biomed. Mater. Res.* **2001**, *55* (2), 203−216.
(146) Skardal, A.; Zhang, J.; Prestwich, G. D. Bioprinting Vessel-like Constructs Using Hyaluronan Hydrogels Crosslinked with Tetrahedral Polyethylene Glycol Tetracrylates. *Biomaterials* **2010**, *31* (24), 6173−6181.
(147) Zhao, Y.; Li, Y.; Mao, S.; Sun, W.; Yao, R. The Influence of Printing Parameters on Cell Survival Rate and Printability in Microextrusion-Based 3D Cell Printing Technology. *Biofabrication* **2015**, *7* (4), 045002.
(148) Lee, J. U.; Yeo, M.; Kim, W. J.; Koo, Y. W.; Kim, G. H. Development of a Tannic Acid Cross-Linking Process for Obtaining 3D Porous Cell-Laden Collagen Structure. *Int. J. Biol. Macromol.* **2018**, *110*, 497.
(149) Shim, J. H.; Lee, J. S.; Kim, J. Y.; Cho, D. W. Bioprinting of a Mechanically Enhanced Three-Dimensional Dual Cell-Laden Construct for Osteochondral Tissue Engineering Using a Multi-Head Tissue/Organ Building System. *J. Micromech. Microeng.* **2012**, *22*, 085014.
(150) Li, C.; Faulkner-Jones, A.; Dun, A. R.; Jin, J.; Chen, P.; Xing, Y.; Yang, Z.; Li, Z.; Shu, W.; Liu, D.; Duncan, R. R. Rapid Formation of a Supramolecular Polypeptide-DNA Hydrogel for in Situ Three-Dimensional Multilayer Bioprinting. *Angew. Chem., Int. Ed.* **2015**, *54*, 3957.
(151) Miranda, P.; Pajares, A.; Saiz, E.; Tomsia, A. P.; Guiberteau, F. Mechanical Properties of Calcium Phosphate Scaffolds Fabricated by Robocasting. *J. Biomed. Mater. Res., Part A* **2008**, *85A* (1), 218−227.
(152) Senatov, F. S.; Niaza, K. V.; Zadorozhnyy, M. Y.; Maksimkin, A. V.; Kaloshkin, S. D.; Estrin, Y. Z. Mechanical Properties and Shape Memory Effect of 3D-Printed PLA-Based Porous Scaffolds. *J. Mech. Behav. Biomed. Mater.* **2016**, *57*, 139.
(153) Pfister, A.; Landers, R.; Laib, A.; Hübner, U.; Schmelzeisen, R.; Mülhaupt, R. Biofunctional Rapid Prototyping for Tissue-Engineering Applications: 3D Bioplotting versus 3D Printing. *J. Polym. Sci., Part A: Polym. Chem.* **2004**, *42* (3), 624−638.
(154) Luo, Y.; Luo, G.; Gelinsky, M.; Huang, P.; Ruan, C. 3D Bioprinting Scaffold Using Alginate/Polyvinyl Alcohol Bioinks. *Mater. Lett.* **2017**, *189*, 295−298.
(155) Wu, Z.; Su, X.; Xu, Y.; Kong, B.; Sun, W.; Mi, S. Bioprinting Three-Dimensional Cell-Laden Tissue Constructs with Controllable Degradation. *Sci. Rep.* **2016**, *6* (1), 24474.
(156) Temple, J. P.; Hutton, D. L.; Hung, B. P.; Huri, P. Y.; Cook, C. A.; Kondragunta, R.; Jia, X.; Grayson, W. L. Engineering Anatomically Shaped Vascularized Bone Grafts with HASCs and 3D-Printed PCL Scaffolds. *J. Biomed. Mater. Res., Part A* **2014**, *102* (12), 4317−4325.
(157) Lee, J. W.; Choi, Y. J.; Yong, W. J.; Pati, F.; Shim, J. H.; Kang, K. S.; Kang, I. H.; Park, J.; Cho, D. W. Development of a 3D Cell Printed Construct Considering Angiogenesis for Liver Tissue Engineering. *Biofabrication* **2016**, *8*, 015007.
(158) Serra, T.; Planell, J. A.; Navarro, M. High-Resolution PLA-Based Composite Scaffolds via 3-D Printing Technology. *Acta Biomater.* **2013**, *9* (3), 5521−5530.
(159) Jakus, A. E.; Rutz, A. L.; Jordan, S. W.; Kannan, A.; Mitchell, S. M.; Yun, C.; Koube, K. D.; Yoo, S. C.; Whiteley, H. E.; Richter, C. P.; Galiano, R. D.; Hsu, W. K.; Stock, S. R.; Hsu, E. L.; Shah, R. N. Hyperelastic "Bone": A Highly Versatile, Growth Factor-Free, Osteoregenerative, Scalable, and Surgically Friendly Biomaterial. *Sci. Transl. Med.* **2016**, *8*, 358ra127.
(160) Bakarich, S. E.; Gorkin, R.; Panhuis, M. i. h.; Spinks, G. M. 4D Printing with Mechanically Robust, Thermally Actuating Hydrogels. *Macromol. Rapid Commun.* **2015**, *36*, 1211.
(161) Soltan, N.; Ning, L.; Mohabatpour, F.; Papagerakis, P.; Chen, X. Printability and Cell Viability in Bioprinting Alginate Dialdehyde-Gelatin Scaffolds. *ACS Biomater. Sci. Eng.* **2019**, *5* (6), 2976−2987.

https://doi.org/10.1021/acsbiomaterials.1c00598
ACS Biomater. Sci. Eng. XXXX, XXX, XXX−XXX

(162) Habib, A.; Khoda, B. Development of Clay Based Novel Hybrid Bio-Ink for 3D Bio-Printing Process. *J. Manuf. Process.* **2019**, *38*, 76−87.
(163) Habib, A.; Sathish, V.; Mallik, S.; Khoda, B. 3D Printability of Alginate-Carboxymethyl Cellulose Hydrogel. *Materials* **2018**, *11*, 454.
(164) Webb, B.; Doyle, B. J. Parameter Optimization for 3D Bioprinting of Hydrogels. *Bioprinting* **2017**, *8*, 8−12.
(165) Cheng, Z.; Cui, M.; Shi, Y.; Qin, Y.; Zhao, X. Fabrication of Cell-Laden Hydrogel Fibers with Controllable Diameters. *Micromachines* **2017**, *8*, 161.
(166) Thattaruparambil Raveendran, N.; Vaquette, C.; Meinert, C.; Samuel Ipe, D.; Ivanovski, S. Optimization of 3D Bioprinting of Periodontal Ligament Cells. *Dent. Mater.* **2019**, *35* (12), 1683−1694.
(167) Daly, A. C.; Critchley, S. E.; Rencsok, E. M.; Kelly, D. J. A Comparison of Different Bioinks for 3D Bioprinting of Fibrocartilage and Hyaline Cartilage. *Biofabrication* **2016**, *8* (4), 045002.
(168) Giuseppe, M. Di; Law, N.; Webb, B.; Macrae, R. A.; Liew, L. J.; Sercombe, T. B.; Dilley, R. J.; Doyle, B. J. Mechanical Behaviour of Alginate-Gelatin Hydrogels for 3D Bioprinting. *J. Mech. Behav. Biomed. Mater.* **2018**, *79*, 150−157.
(169) De Witte, T.-M.; Fratila-Apachitei, L. E.; Zadpoor, A. A.; Peppas, N. A. Bone Tissue Engineering via Growth Factor Delivery: From Scaffolds to Complex Matrices. *Regen. Biomater.* **2018**, *5* (4), 197−211.
(170) Wu, T.; Yu, S.; Chen, D.; Wang, Y. Bionic Design, Materials and Performance of Bone Tissue Scaffolds. *Materials* **2017**, *10*, 1187.
(171) Hutmacher, D. W. Scaffolds in Tissue Engineering Bone and Cartilage. *Biomaterials* **2000**, *21* (24), 2529−2543.
(172) Wells, R. G. Tissue Mechanics and Fibrosis. *Biochim. Biophys. Acta, Mol. Basis Dis.* **2013**, *1832* (7), 884−890.
(173) Sweigart, M. A.; Zhu, C. F.; Burt, D. M.; deHoll, P. D.; Agrawal, C. M.; Clanton, T. O.; Athanasiou, K. A. Intraspecies and Interspecies Comparison of the Compressive Properties of the Medial Meniscus. *Ann. Biomed. Eng.* **2004**, *32* (11), 1569−1579.
(174) Mostafavi, A.; Abudula, T.; Russell, C. S.; Mostafavi, E.; Williams, T. J.; Salah, N.; Alshahrie, A.; Harris, S.; Basri, S. M. M.; Mishra, Y. K.; Webster, T. J.; Memic, A.; Tamayol, A. In Situ Printing of Scaffolds for Reconstruction of Bone Defects. *Acta Biomater.* **2021**, *127*, 313.
(175) Quint, J. P.; Mostafavi, A.; Endo, Y.; Panayi, A.; Russell, C. S.; Nourmahnad, A.; Wiseman, C.; Abbasi, L.; Samandari, M.; Sheikhi, A.; Nuutila, K.; Sinha, I.; Tamayol, A. In Vivo Printing of Nanoenabled Scaffolds for the Treatment of Skeletal Muscle Injuries. *Adv. Healthcare Mater.* **2021**, *10*, 2002152.
(176) Ma, K.; Zhao, T.; Yang, L.; Wang, P.; Jin, J.; Teng, H.; Xia, D.; Zhu, L.; Li, L.; Jiang, Q.; Wang, X. Application of Robotic-Assisted in Situ 3D Printing in Cartilage Regeneration with HAMA Hydrogel: An in Vivo Study. *J. Adv. Res.* **2020**, *23*, 123−132.
(177) Urciuolo, A.; Poli, I.; Brandolino, L.; Raffa, P.; Scattolini, V.; Laterza, C.; Giobbe, G. G.; Zambaiti, E.; Selmin, G.; Magnussen, M.; Brigo, L.; De Coppi, P.; Salmaso, S.; Giomo, M.; Elvassore, N. Intravital Three-Dimensional Bioprinting. *Nat. Biomed. Eng.* **2020**, *4* (9), 901−915.

https://doi.org/10.1021/acsbiomaterials.1c00598
ACS Biomater. Sci. Eng. XXXX, XXX, XXX−XXX